




Article

Dynamic-Based Limit Analysis for Seismic Assessment of Free-Standing Walls of San Giovanni Church in Castelseprio UNESCO World Heritage Site

Luca Sbrogiò ^{1,*} , Lorenzo Tavano ², Ylenia Saretta ¹ , Amedeo Caprino ³, Alejandra Chavarría Arnau ¹, Gian Pietro Brogiolo ⁴ and Maria Rosa Valluzzi ¹ 

¹ Department of Cultural Heritage, University of Padova, Piazza Capitaniato 7, 35139 Padova, Italy

² Department of Civil Environmental and Architectural Engineering, University of Padova, Via F. Marzolo 9, 35131 Padova, Italy

³ Department of Geosciences, University of Padova, Via Gradenigo 6, 35131 Padova, Italy

⁴ University of Padova, Piazza Capitaniato 7, 35139 Padova, Italy

* Correspondence: luca.sbrogio@unipd.it; Tel.: +39-049-827-5386

Abstract: Free-standing archaeological walls are significantly exposed to horizontal actions (e.g., earthquakes) as they lack connections provided by floors or roofs. In such cases, the dynamic response governs the activation of local mechanisms of collapse, determining the shape of the macroblocks and their position. Engineering models of archaeological walls are developed according to the results of extensive visual inspections and on-site testing, including modal identification for calibration purposes. A modal response spectrum analysis on the calibrated model identifies the zones where the tensile stress is exceeded, which are more likely to detach as rigid macroblocks and subsequently overturn due to the expected ground spectra. The macroblocks are then assessed according to limit analysis. The case studies are the north and the apse walls of the church of San Giovanni Evangelista in Castelseprio (Varese, Lombardy), a 5th century Longobard fortified settlement, a part of UNESCO World Heritage. The construction quality of the apse was poorer than the north wall, but the masonry of both is very compact thanks to the good mortar. The macroblocks are identified mostly in the upper crests of the walls, and their acceleration of activation is two to six times larger than the demand (considering the dynamic amplification that the structure applies to the ground motion); therefore, no particular intervention is needed. The proposed method will require additional calibration, e.g., through nonlinear dynamic analyses, and a more precise treatment of uncertainties in masonry mechanical properties to determine the shape of the macroblocks.

Keywords: early middle ages; archaeological site; on-site testing; limit analysis; masonry; dynamic behavior; response spectrum analysis



Citation: Sbrogiò, L.; Tavano, L.; Saretta, Y.; Caprino, A.; Chavarría Arnau, A.; Brogiolo, G.P.; Valluzzi, M.R. Dynamic-Based Limit Analysis for Seismic Assessment of Free-Standing Walls of San Giovanni Church in Castelseprio UNESCO World Heritage Site. *Heritage* **2024**, *7*, 448–475. <https://doi.org/10.3390/heritage7010022>

Academic Editors: Humberto Varum, Vasilis Sarhosis and Fernanda Prestileo

Received: 7 December 2023

Revised: 10 January 2024

Accepted: 11 January 2024

Published: 18 January 2024



Copyright: © 2024 by the authors. Licensee MDPI, Basel, Switzerland. This article is an open access article distributed under the terms and conditions of the Creative Commons Attribution (CC BY) license (<https://creativecommons.org/licenses/by/4.0/>).

1. Introduction

Archaeological sites are an important part of cultural heritage, providing the link between modern society and past civilizations and allowing an understanding of their organization. Their conservation, through proper maintenance [1], and protection from both natural and human-induced risks [2,3], through well-designed interventions, are of paramount importance, on the one side, enabling future research and, on the other, allowing visitors onto the site in safe conditions.

Archaeological structures, like heritage buildings, may have been exposed to the natural environment for centuries, showing satisfactory behavior. However, a proper assessment of the safety levels is required, especially when brittle failure mechanisms are expected, such as local mechanisms of collapse [4]. The heterogeneous nature of remains adds complexity to their assessment and requires approaches tailored for each case, albeit in the framework of acknowledged procedures [5–7]. These recommend that qualitative

evaluations complete and guide the tests and the quantitative assessment, as well as that the experience of the site/building contributes to the understanding of its behavior [1,8,9].

Archaeological structures also lack the fundamental prerequisites for distributing seismic forces effectively: free-standing elements, without horizontal diaphragms, possess minimal restraint against horizontal forces, hindering the attainment of box-like behavior. In such cases, structural dynamics govern the response [10], and mode shapes induce local amplification in single walls or building elements, such as parapets or pediments [11]. These local peaks in acceleration lead to stress concentration and abnormal displacements, which can cause cracks, thus influencing the activation of local mechanisms [12].

Therefore, the seismic assessment of archaeological structures can be carried out either through the study of equivalent static equilibrium of masonry walls [13,14], i.e., limit analysis, or by considering the rocking behavior as a response to a dynamic input on detailed numerical models, e.g., discrete element (DE) ones [15–17]. As DE modeling is better suited to block-based structures, where friction governs block-to-block contact [18], its widespread application to masonry structures may be not feasible, especially in the case of random rubble masonry walls [19]. Conversely, limit analysis offers a general and simplified method for studying the equilibrium of substructures within masonry buildings, typically walls or portions thereof, which are schematized as rigid bodies (macroblocks) hinged or supported at their ends [20,21]. In this method, horizontal forces act where the strength of the system is the weakest, i.e., perpendicular to the wall plane (out-of-plane overturning), and plastic hinges appear where the (small) tensile stress of masonry is exceeded [4,21]. This approach is commonly applied to historic unreinforced masonry buildings due to its simple depiction of a common structural behavior [22]. However, by ignoring the dynamic response of a structure, two main limitations affect the representativeness of this method: (i) macroblocks are identified conventionally, often coinciding with entire walls; (ii) the position of hinges is also conventionally determined by placing them at external constraints (ground, floors, and other structures). The importance of the dynamic response of masonry buildings is now widely recognized in assessment procedures to detect damage [23] and possible local mechanisms [24].

2. Materials and Methods

2.1. Methodological Approach

The general framework of the paper follows the criteria proposed by [5,25] and by other engineering studies specifically focusing on archaeological sites [13,26–28]; the calculation method for the safety assessment is also well known, being that of limit analysis [4,20]. The main novelty of the procedure stays in the study of the dynamic behavior of archaeological structures through a modal response spectrum analysis (MRSA) to determine (i) the type of local mechanism of collapse, (ii) the shape of the macroblocks, and (iii) the seismic acceleration that impacts on them. Particular care was put in both cross-checking the results of on-site tests and using them in structural modeling. Considering the needs of the programmed conservation of architectural heritage [29], this procedure can be further extended to the definition of informative models or digital twins [30].

The approach here proposed considers three macro-phases, i.e., the exploratory study, the structural modeling, and the safety assessment (Figure 1). The exploratory study involves: (i) geometric survey, which determines the overall dimensions of the loadbearing structures; (ii) visual inspections, which aim at qualifying materials and assessing their preservation state; (iii) on-site testing, focused on estimating the mechanical properties of building materials [6]. The study of historical documentation and archaeological excavations is a fundamental premise to these operations [5,31]. The results of the exploratory study determine the choice of the structural model and provide its input values (macro-phase 2). Once the structural scheme is defined, they also serve as a check for its reliability, by recursively updating the relevant mechanical properties until a calibrated model is obtained. The safety assessment (macro-phase 3) relies on a structural analysis that must

be suited for the type of structure considered and the actions expected on it. Depending on the safety levels obtained, simple maintenance or interventions can be programmed [1].

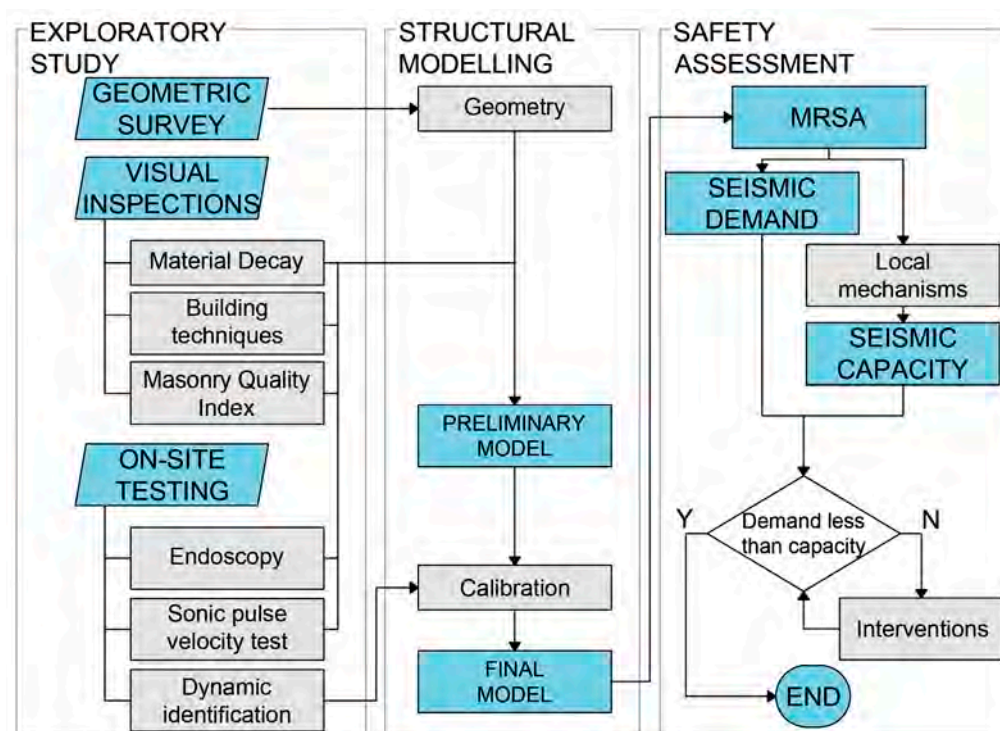


Figure 1. Workflow of the engineering methodological approach to an archaeological site proposed in this work.

2.1.1. Exploratory Study

Laser scanners and drones are nowadays indispensable tools for geometric surveys of architectural heritage [32,33], but the latter are particularly useful in archaeological sites, as they can cover vast areas and obtain both the plans of the excavation and the elevations of the standing walls. In addition, close-up images of the walls are instrumental for several studies involving visual inspections (the analysis of building techniques [34], the stratigraphy of building elevations [35], and the masonry quality index (MQI) [36]) and for assessing the preservation state of the edges of the walls, which are more exposed to material degradation and may be difficult to see from the ground.

Archaeological analyses of elevations aim at detecting changes in masonry arrangement and discontinuities within masonry textures, which may be the result of either different building phases or different construction practices. Structurally, these features are associated with the concentration or generation of seismic damage [37].

The MQI is a method that involves assessing seven criteria that are connected with the internal arrangement of a wall, both in its elevation and cross-section [36,38]. Its usage is also suggested by the Italian seismic code [6], and it has been already applied to heritage buildings [39,40]. Each criterion is evaluated by a score ranging from 0 to 2 from the lowest to the highest compliance with an ideal ‘rule of thumb’, which ensures the strength and compactness of a wall in respect to vertical (MQI_V) and in-plane (MQI_{IP}) or out-of-plane (MQI_{OOP}) horizontal loads that may arise during earthquakes. The three indexes, one for each action, are obtained as a linear combination of the scores, as described by [36].

The ranges of the three indices and the corresponding quality category are given in Table 1: masonry walls with an A outcome are compact and can withstand earthquake loads with negligible or slight damage, whereas those with a C rating have minimum strength and reach failure generally through disaggregation [41].

Table 1. Masonry quality categories according to the results of the MQI in the three main directions of a wall.

Direction	Masonry Quality		
	Poor (Category C)	Mediocre (Category B)	Good (Category A)
Vertical (MQI _V)	0–2.5	2.5–5	5–10
In plane, horizontal (MQI _{IP})	0–4	4–7	7–10
Out of plane, horizontal (MQI _{OOP})	0–3	3–5	5–10

Since this method mainly evaluates the texture of a masonry wall, it can be used in a structure for determining those areas where a similar behavior is expected and for establishing a qualitative hierarchy among different types, when many of them appear either for constructive reasons or because of transformations. In addition, MQIs have been correlated to the main mechanical properties of masonry [39,42], and this can help in categorizing the masonry according to [6] and in giving a rough estimate of its strength for preliminary modeling.

Endoscopic tests (ENDs) and sonic pulse velocity tests (SPVTs) complete this superficial analysis through the direct and indirect inspection of the cross-section of a wall, respectively [6]. ENDs use the images coming from a flexible probe with a light and a camera on top. The probe is inserted into a drilled hole or, in the case of archaeological structures, existing holes, such as those left by scaffolding or cracks [43]. SPVTs qualify the density of a wall by detecting local internal variations, significant inclusions, and voids [44,45], and, being a non-destructive test, they are suitable for archaeological sites [46,47]. SPVT relies on the transmission of elastic waves with frequencies ranging from 20 to 20,000 Hz (within the range of sound) through a wall [48]. These tests are quick and can explore moderately large portions of a wall, but the results are affected by the instrumentation and the signal propagation in heterogeneous media. Previous research on SPVTs, also comparing their results with the outcomes of other testing methods [49], tentatively described masonry quality density as low when the velocity is less than 1000 m/s and as good when above 2000 m/s, with intermediate situations in between; however, a strong dependency on the nature of stones (porous or compact) and humidity has been recognized in the results.

Finally, the modal analysis of structures studies the dynamic behavior of systems under natural or forced vibrations: such an overall understanding of a structure can compensate for the local nature of the tests previously mentioned. Modal analysis provides information about natural frequencies, modal shapes (how the structure moves at certain frequencies), and damping coefficients. Operational modal analysis (OMA) utilizes environmental forces (wind, traffic, and microtremors) as the source of excitation and offers the possibility of analyzing a structure with minimal impact (temporary and pointwise sensor attachment) and, in its actual operating conditions, making it particularly suitable for cultural heritage buildings [50–53] and archaeological sites [54,55]. In order to reduce errors in the identification of dynamic parameters, the recorded acceleration time series can be processed both in frequency and time domain. The frequency domain analyses include enhanced frequency domain decomposition (EFDD) [56] and the poly-reference least squares complex frequency domain (pLSCF) [57], whereas considering the time-domain techniques, stochastic subspace identification (SSI) is the most common [58]. The EFDD and the SSI are implemented in ARTEMIS software (version 6.0) [59], but the pLSCF is implemented in MACEC (version 3.4) [60].

2.1.2. Structural Modeling

The numerical modeling approach proposed in this study involves the utilization of a 3D continuous finite elements (FE) model. Specifically, four-node shell elements are employed, aligned with the middle plane of the walls and assuming homogeneous equivalent mechanical properties, according to the macro-modeling approach for masonry [61].

Although 3D brick elements are in use for the modeling of masonry structures, shell elements are still a good compromise between precision and calculation demands [62,63]. In addition, the calibration and the analyses carried out in the following are all referred to the linear field, so the usage of simpler elements is still reliable. In defining the model, those areas identified as homogeneous according to visual inspections and the MQI method received specific preliminary mechanical properties by converting the MQI values with the formulations provided by [42]. The sonic velocity, obtained from SPVTs, contributes to determining the preliminary local density of the masonry, as the MQIs are correlated just to its strength and elasticity parameters.

Once the numerical model is set up with preliminary properties, it needs to be updated by modifying those that affect the dynamic behavior (i.e., density and elastic moduli) in order to match the OMA results [64,65]. However, the calculation of a sensitivity index for each parameter, S_n (Equation (1)), is needed to assess their relative influences on the response and guide the trials.

$$S_n = \frac{R_{\max} - R_{\min}}{R_{\max} + R_{\min}} \times \frac{P_{\max} + P_{\min}}{P_{\max} - P_{\min}} \quad (1)$$

where R_{\max} and R_{\min} represent the maximum and minimum measured response, while P_{\max} and P_{\min} are the maximum and minimum values considered for the parameter for which the sensitivity index is to be calculated. S_n takes values between 0 and 1 [66], and it is higher as the impact of the associated property variation on the model is greater.

The updating is a recursive procedure [65] that is repeated until numerical outputs are correlated with experimental analysis results either qualitatively, observing modal shapes, or quantitatively. In the latter case, the assessment considers both the relative error ε between frequencies (Equation (2)) [67–69] and the modal assurance criterion (MAC, Equation (3)), which yields a dimensionless value between 0 (no correspondence between two methods, experimental and numerical) and 1 (complete correspondence) [70].

$$\varepsilon = \frac{|f_{i,A} - f_{i,B}|}{f_{i,A}} \times 100 \quad (2)$$

$$MAC_{ij} = \frac{|\sum_{k=1}^n \psi_{ik} \psi_{jk}|^2}{\sum_{k=1}^n (\psi_{ik})^2 \sum_{k=1}^n (\psi_{jk})^2} \quad (3)$$

In Equation (2), $f_{i,A}$ identifies the frequency associated with the i -th mode of method A, and $f_{i,B}$ identifies the frequency associated with the i -th mode of method B. In Equation (3), ψ_{ik} represents the k -th mode shape vector of mode i , while ψ_{jk} represents the k -th mode shape vector of mode j . A good correlation between numerical and experimental modes is expected when the MAC is larger than 0.9 [71].

2.1.3. Seismic Assessment

The seismic assessment uses a linear dynamic analysis, i.e., a modal response spectrum analysis (MRSA, [72]) on the calibrated model, to detect the local mechanisms and then limit analysis for their computation. The overall structural response (displacement, stress, and acceleration) is determined as the square root of the sum of squares (SRSS) or the complete quadratic (CQC) combinations [72] of the MRSA for each main mode of vibration to a seismic ground spectrum S_e .

The analysis returns the elastic stresses in the material but, due to the small tensile strength of masonry f_t , where the principal tensile stresses exceed this value on the tensioned side of a wall, cracks are expected, with the consequent formation of plastic hinges on the compressed side [21] (Figure 2).

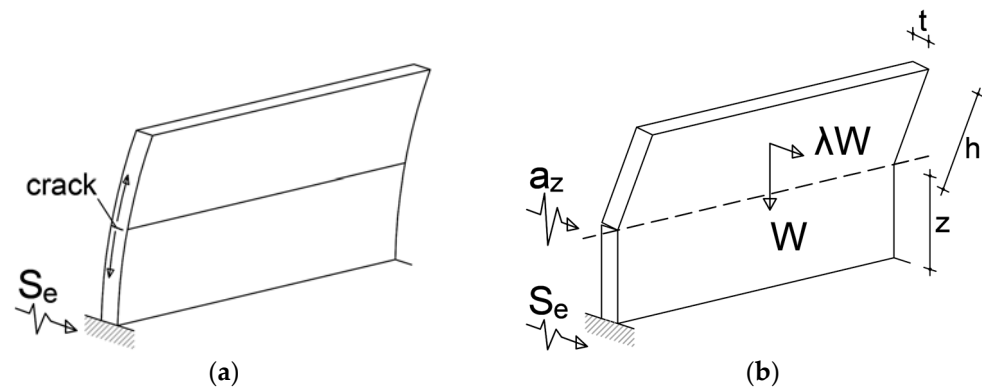


Figure 2. Structural scheme for the computation of local mechanisms: (a) tensile stresses arising in the material due to the vibrations proportional to mode shapes and crack formation; (b) equivalent macroblock and local mechanism: the dashed line represents the position of the plastic hinge on the compressed side. S_e and a_z are response spectra at the ground and hinge level, respectively.

For old masonry types, [6] provides the value of τ_0 , which is the shear strength to diagonal cracking: the tensile strength can be calculated through Equation (4) as proposed by [73]. CF is the confidence factor, which reduces the strength of materials depending on the knowledge level about the structure, as a function of the inspections and the tests [6].

$$f_t = \frac{1.5\tau_0}{CF} \quad (4)$$

The macroblocks involved in the local mechanisms are those parts of the walls above the cracks, where displacements are the largest (Figure 2a). The first position of a wall where the tensile strength is exceeded corresponds to the opening of the cracks, leading to the formation of plastic hinges: the portion above the hinge (where the tensile strength is always exceeded) is the macroblock affected by kinematics, whereas the portion below is considered stable since there is no redistribution of forces (Figure 2b).

Then, the horizontal seismic acceleration (spectral acceleration of activation, a_0^*) that causes the overturning of macroblocks, assuming them to be simply hinged at their base, is calculated according to Equation (5) [6,20]:

$$a_0^* = \frac{\lambda \times \Sigma_i w_i}{M^* \times CF} \quad (5)$$

where λ is the multiplying factor of the horizontal loads that governs the local mechanism, $\Sigma_i w_i$ is the summation of the i -th weight w of the macroblocks involved in the local mechanism, M^* is the equivalent participating mass of the system [6], and CF accounts for the uncertainties that affect the activation. However, if the simple overturning of a single macroblock, hinged at its base, is considered (Figure 2b), $\lambda = t/h$, the total weight $\Sigma_i w_i$ of the system coincides with the weight of the macroblock $w = mg$, and the participant mass coincides with the mass m of macroblock. With these replacements, Equation (5) can be rewritten as Equation (6).

$$a_0^* = \frac{t \times \Sigma_i w_i}{h \times m \times CF} = \frac{t \times g}{h \times FC} \quad (6)$$

The reduction in a_0^* to account for the initial dynamic response of the macroblock [20] is generally very small, and therefore, it will be neglected in the following.

The average acceleration a_z acting at the hinge level z , due to the dynamic amplification of the ground motion S_e , is determined from the MRSA. This is an alternative approach to the calculation of response spectra at the intermediate levels of a structure, as proposed by [11]. Finally, a_0^* and a_z are compared for the safety check, which is satisfied when $a_0^* \geq a_z$.

As a linear verification, in the Italian code, a_0^* is compared to either damage limitation (DL) or no-collapse (NC) limit states, provided that this latter is divided by behavior factor q , both for the spectra at the ground and at an intermediate level of the structure [6]. Actually, the activation of local mechanisms is an intermediate condition between the DL and NC limit states [74]. Therefore, the procedure here presented is repeated considering in the MRSA both the expected DL and NC ground spectra defined by the Italian code for the site of the assessment.

2.2. Case Study

This case study is S. Giovanni Evangelista, the parish church of Castelseprio, a settlement that was recognized in 2011 as a UNESCO World Heritage site, along with other sites in Italy, as an evidence of the Longobard presence between the 6th and the 8th centuries. After excavations and studies carried out in the middle 20th century, since 2022, a unitary research project has promoted new studies on S. Giovanni and on the other buildings of the site, reconsidering historical documentation and carrying out new excavations and geometric surveys of the site by means of drones [75].

The area of Castelseprio is one of the least seismically active in Italy, with very few historical records and macroseismic intensities not exceeding degree 5 [76,77]. However, some traces in S. Giovanni and in the other main buildings of the site, both destroyed and still standing [78], may be explained by some past seismic activity. Further research is still ongoing on this subject, but in the following, just the assessment of the surviving parts of S. Giovanni in their present state will be discussed.

2.2.1. Description

The church of San Giovanni is part of a Christian complex that includes a basilica, a monumental baptistery, a tower, and a cistern (Figure 3).

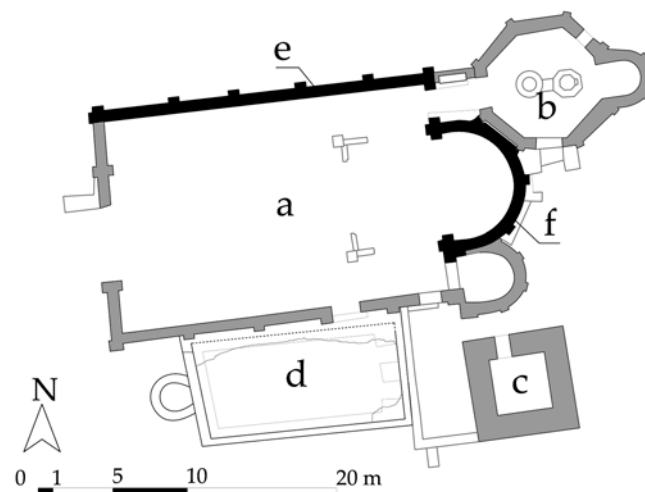


Figure 3. Plan of the S. Giovanni complex. The letters mark: (a) church; (b) baptistery; (c) bell tower; (d) cistern; (e) north wall; (f) main apse (adapted from [79]). The walls studied in this paper are marked in black.

Historical records indicate that the church, built in the 6th or 7th century, was spared from the demolition of the settlement ordered in 1287 by Milanese troops, and it was continuously used for liturgical and funerary purposes at least until the 14th century [78]. After that, the church gradually fell into disrepair and abandonment, ultimately becoming a ruin [75].

Currently, the state of preservation of the surviving walls varies significantly. The facade has almost entirely disappeared, leaving behind scant remnants. The side walls stand preserved up to approximately 5 m in height, while the apse section remains relatively

intact, reaching a height of nearly 10 m (Figures 4 and 5). In contrast, the walls of the baptistery have a uniform height just above 1 m, suggesting intentional demolition [75].

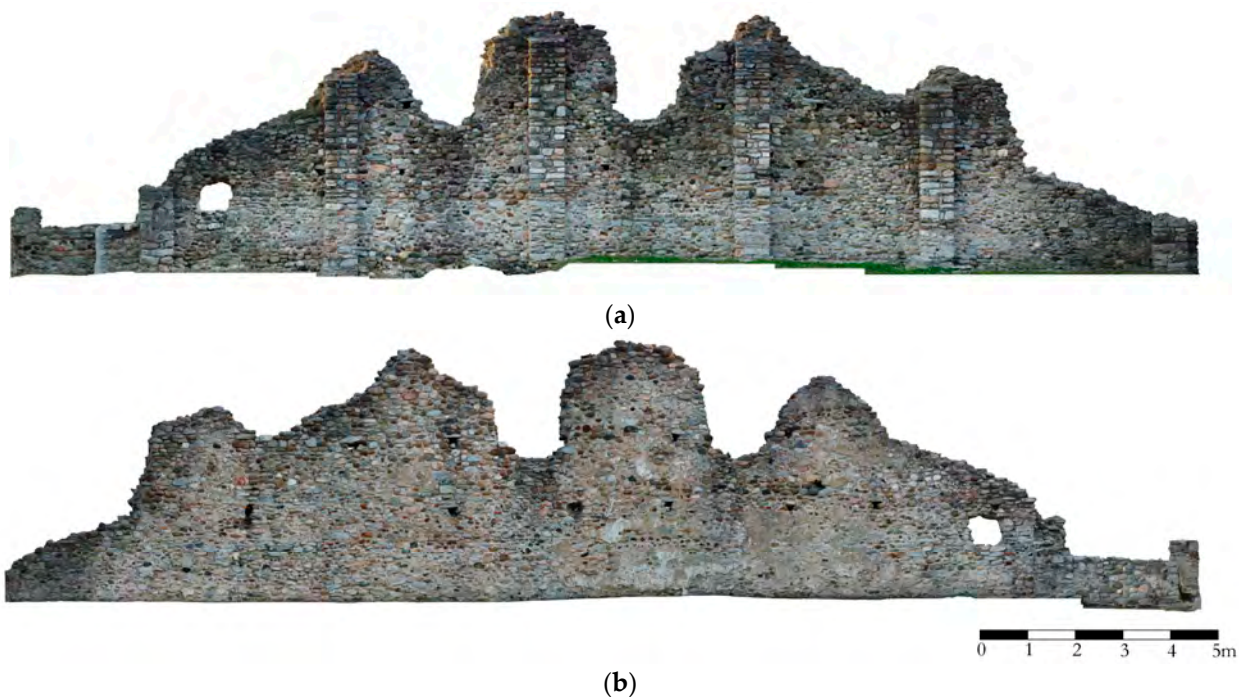


Figure 4. Church of S. Giovanni; elevations of the north wall: (a) external; (b) internal (credits: P. Vedovetto, adapted from [79]).



Figure 5. Church of S. Giovanni; elevation of the main apse: (a) external; (b) internal (credits: P. Vedovetto, adapted from [79]).

Bishops' visits and archaeological investigations revealed that the parish church had been divided into three aisles, but just the foundations of the pillars were found. The main apse measures 6.45 m in chord length by 5.16 m in depth, while the north wall is about 23 m long; wall thickness ranges between 70 and 75 cm. The apse windows occupy just the southern half of the basin, and this, with other stratigraphical traces, causes [79] to suppose that it was built, along with the church, after the construction of the baptistery. The perimeter walls and apses are marked by half pilasters (Figure 6a), but there is not a perfect match in the scanning of the north and the south walls. The buttresses and the fillings that now block the windows in the apse (Figure 6b), along with other clues on the other walls,

have been attributed to repairs following an earthquake (Verona 1117, according to [79]), but additional research is expected in this regard.

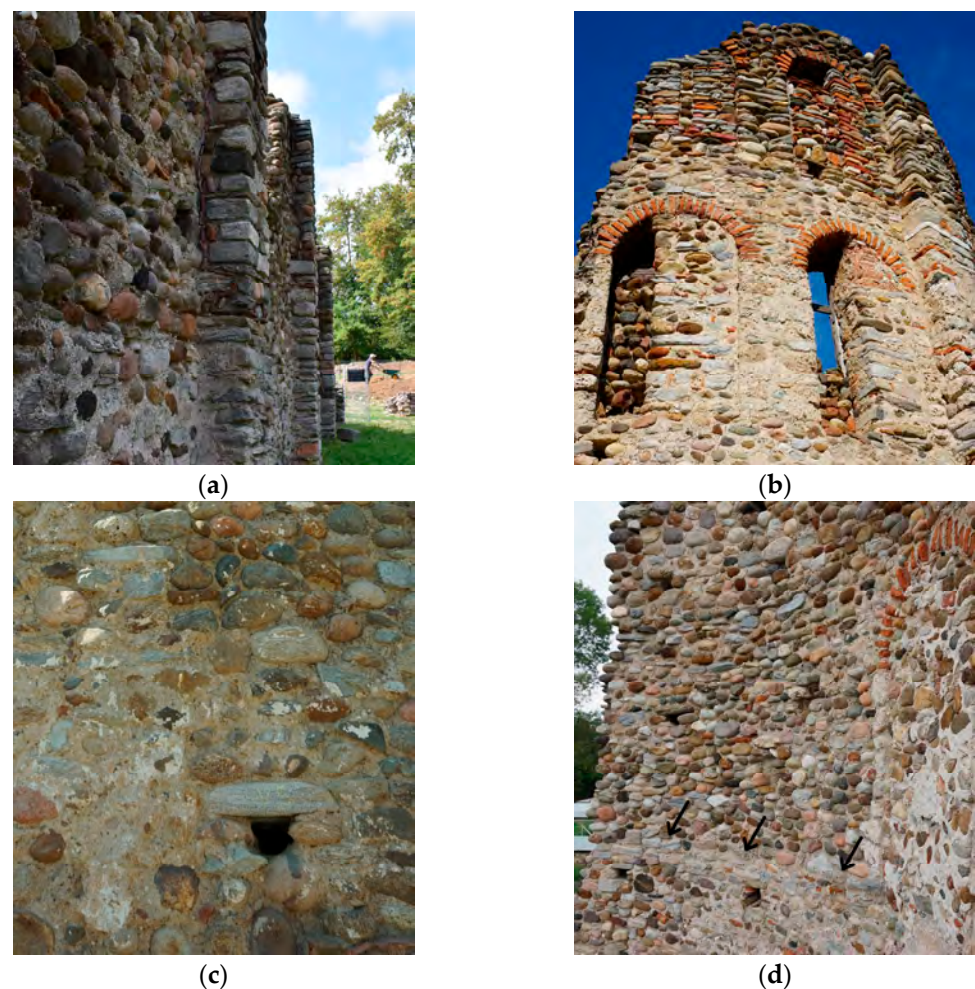


Figure 6. Constructive details of S. Giovanni: (a) half pilasters along the north wall with tile fragments bordering the integrated parts; (b) blocked windows and buttresses added onto the apse (from the outside); (c) scaffolding holes in the apse; (d) horizontal joint connected to a construction stage in the apse (black arrows).

During restorations undertaken in the mid-20th century, the rebuilt parts were demarcated by brick and tile fragments, notably visible in the half-pilasters lining the walls (Figure 6a), whereas in the 1990s, the upper crests were sealed with epoxy injections [80]. However, neither the extent of the interventions nor the type of resins is known.

2.2.2. Building Techniques

The masonry is constructed using pebbles, rough ashlar, and slabs of various types (igneous, metamorphic, and sedimentary), sourced from the riverbed of the nearby Olona River [80]. The pebbles range in size from 3 to 40 cm and are used for building the masonry mass; smaller ones are employed as gallets to reduce mortar gaps. Rough ashlar and slabs reach lengths of 60–100 cm and are located near the corners of the building, in the half-pilasters (Figure 6a), or above the scaffolding holes (Figure 6c). Bricks are mainly found in the arches and in the infill of the apse windows (Figure 6b), and they come from fragments of Roman sesquipedal bricks and roof tiles [79]. The piers of these windows are built with blocks of spongy travertine, locally quarried [80].

A detailed study of the mortars used in the elevations of San Giovanni is still lacking; however, some conclusions can be drawn from previous studies [80] and by comparing

observations in other buildings on the site and the tombs [81]. It appears that the lime mortar was enriched with pozzolanic reagents, such as clay or crushed pottery, which significantly improved its binding capabilities [82].

The north wall shows a horizontal segmentation at approximately 1.40 m above ground, probably as a result of a construction stage. Both the elements and the mortar joints are smaller below this line than above it. Additionally, roughly hewn stones and small-sized pebbles, which are present in the lower portion, are replaced by larger units. Similarly, in the apse, a horizontal division is visible at a height of 3.40 m above ground, at the level of the second order of windows (Figure 6d). Pebbles are present in both construction stages, but as in the north wall, they are smaller in the lower one.

3. Results

3.1. On-Site Investigations

Following a preliminary inspection of the site, an investigation plan (Figure 7) was drafted with the aim of examining the north wall and the main apse of the church of San Giovanni. The plan included six endoscopies, three in the north wall and three in the main apse, seven MQI analyses, four in the north wall and three in the apse, four SPVTs, two for each investigated structure, and two dynamic identifications, one per each wall. In Figure 7, the MQI analyses and the SPVTs are represented by rectangles that reproduce, in scale, the actual dimensions of the window tested on the walls: MQI requires a $1 \times 1 \text{ m}^2$ window, while the windows for the SPVTs are 0.80 m wide for a height variable between 1.00 m and 1.40 m. The window in test SON2 was reduced to a line due to constraints in the available space.

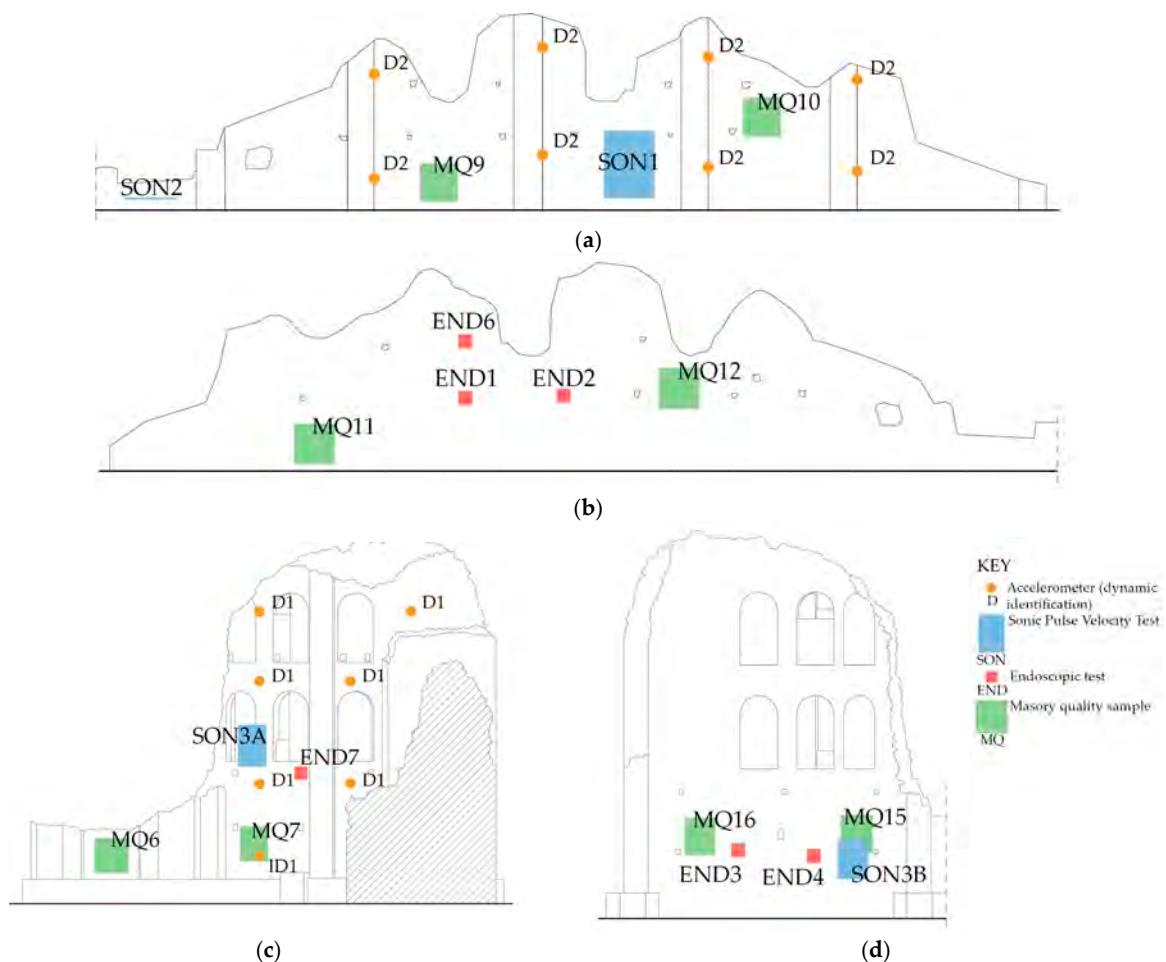


Figure 7. Investigation plan for the walls of S. Giovanni: (a) north wall, external elevation; (b) north wall, internal elevation; (c) main apse, external elevation; (d) main apse, internal elevation.

3.1.1. Visual Inspections and MQI

On-site visual analysis confirmed the recognition of at least three types of mortars (Figure 8): one light grey, used in the perimeter walls, with a clay component [81]; one brownish, probably due to the presence of crushed pottery [80]; and one in dark grey, of cementitious nature and used in modern restorations. All these mortars appeared to be very compact and adherent to the stones, and no signs of disaggregation were detected. The brownish mortar was found in the apse wall, whereas the other two types in the north wall.

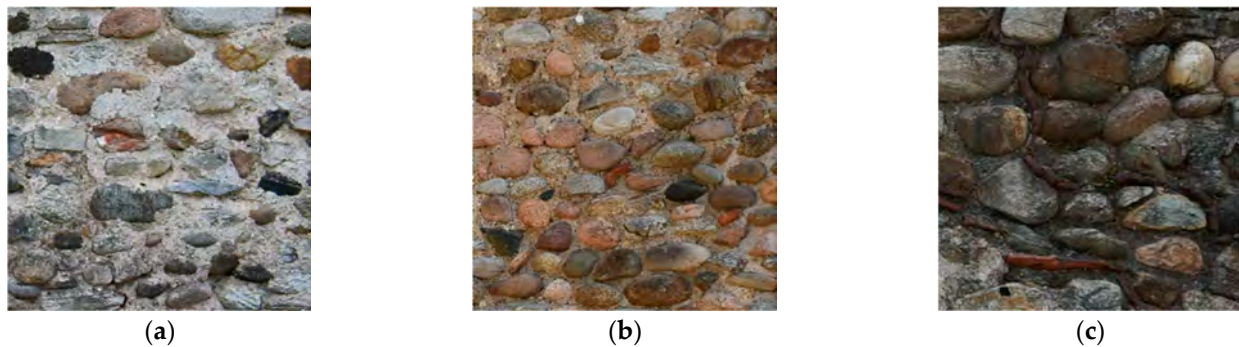


Figure 8. Mortar types in S. Giovanni: (a) lime and clay; (b) lime and crushed pottery; (c) cement.

Overall, both walls exhibited a good preservation state, albeit displaying signs of weathering and alteration in the upper sections and those that are exposed northward.

The masonry quality assessment obtained very poor results (Table 2). The north wall samples (MQ9, MQ10, MQ11, and MQ12, Figure 7a,b) typically received a category B rating for vertical actions (i.e., mediocre quality, see Table 1), except for sample MQ12, which obtained a category C (poor quality) together with the apse samples (MQ7, MQ15, and MQ16, Figure 7c,d). Regarding horizontal actions (both out-of-plane and in-plane), the MQI did not exceed 2.5, and the samples were consistently rated as C. The samples taken from the apse (MQ7, MQ15, and MQ16) demonstrated even lower values of MQI (<2) than the north wall.

Table 2. MQIs for the samples in S. Giovanni (compare the ranges provided in Table 1 for reference).

Sample	Masonry Quality Indices					
	Vertical		Out-of-Plane		In-Plane	
	Category	MQI _V	Category	MQI _{OOP}	Category	MQI _{IP}
MQ9	B	3	C	1.5	C	2.5
MQ10	B	3	C	2.5	C	2.5
MQ11	B	3	C	2	C	2.5
MQ12	C	2	C	2	C	2
MQ7	C	1	C	0.5	C	0.5
MQ15	C	1	C	0.5	C	0.5
MQ16	C	2	C	1.5	C	1

The poor outcomes are motivated mainly by the texture of these walls, as pebbles are considered inadequate for building a good-quality wall, i.e., with continuous and thin horizontal joints, flat-surfaced units, and good staggering. Indeed, mortar joints were as thick as 3–4 cm and represented 35–51% of a 1 × 1 m surface in the north wall, and 43–55% in the apse. However, ENDS showed no sign of an internal infill. This, along with the high compactness of the mortar, makes the masonry behave like a conglomerate rather than as ‘two layers with internal infill’, as it would be described by MQI and the Italian code [6].

3.1.2. Sonic Pulse Velocity Tests

The features of the SPVTs are listed in Table 3. The wall tested in SON2 had a thickness of 110 cm due to the juxtaposition of a tomb in front of the wall.

Table 3. Features of SVPTs in the walls of S. Giovanni.

Test ID	Average Velocity (m/s)	Wall Thickness (cm)	Hammer Side	Grid Rows × Cols	Height from Ground (cm)	Spacing (cm)
SON1	1749	70	Outside	10 × 8	30	20
SON2	1026	110	Outside	1 × 9	40	20
SON3A	642	70	Outside	7 × 5	390	20
SON3B	1235	70	Inside	6 × 5	90	20

The tools and the procedure for data acquisition and subsequent processing of the signals are presented by [83]. For each position in the grids, the velocity is assumed as the average of three measures, and then, the values are interpolated to obtain a contour map.

In the north wall, the SON1 test (Figure 9a) revealed two distinct regions within the sample area, with velocities indicating a decreasing level of compactness from bottom ($v = 2124$ m/s) to top ($v = 1446$ m/s); the overall average velocity of 1749 m/s corresponded to middle-quality masonry in terms of compactness. The average velocity in the SON2 test was 1026 m/s, indicating a masonry wall with many internal voids. The presence of a tomb in this area might have affected the surrounding masonry, potentially creating voids. The SON3A test (Figure 9b) recorded the lowest velocities ($v = 642$ m/s), as it encountered heterogeneous materials, i.e., the pillars made of soft stones and the infill of a window and its sill. Some grid points could not be acquired in the infill, and the minimum velocity ($v = 340$ m/s) was assigned; in the lower part, the values increased to 800–1300 m/s, suggesting a low density, with voids and a poor condition of mortar. The pillars exhibited velocities not exceeding 800–900 m/s, confirming the porosity of the medium. Finally, the SON3B test (Figure 9c), at the base of the apse, revealed a higher average sonic velocity (1235 m/s) and, thus, a higher compactness than the upper part.

It is worth noting that the lower velocities were obtained in those parts that are still or were in the past much more exposed to degradation by percolation of rain, i.e., the upper part of the north wall and the sill of the apse windows and those that were generally cheaply built, i.e., the infill of windows. Indeed, the walls had been partially covered by the ground until the mid-20th century.

3.1.3. Dynamic Identification

Eight piezometric accelerometers were placed according to a triangular grid pattern on the external face of the north wall, while seven accelerometers were installed on the southern half of the central apse due to limitations imposed by the adjacent baptistery wall and its shelter roof (Figure 10a). The sensors were temporarily affixed with hot glue, for avoiding drilling into the archaeological material, and were cable-connected to an acquisition system, recording signals at 10 min intervals over an hour (Figure 10b). They were applied on the external side of both structures, as the interior of the church is occupied by the archaeological excavations.

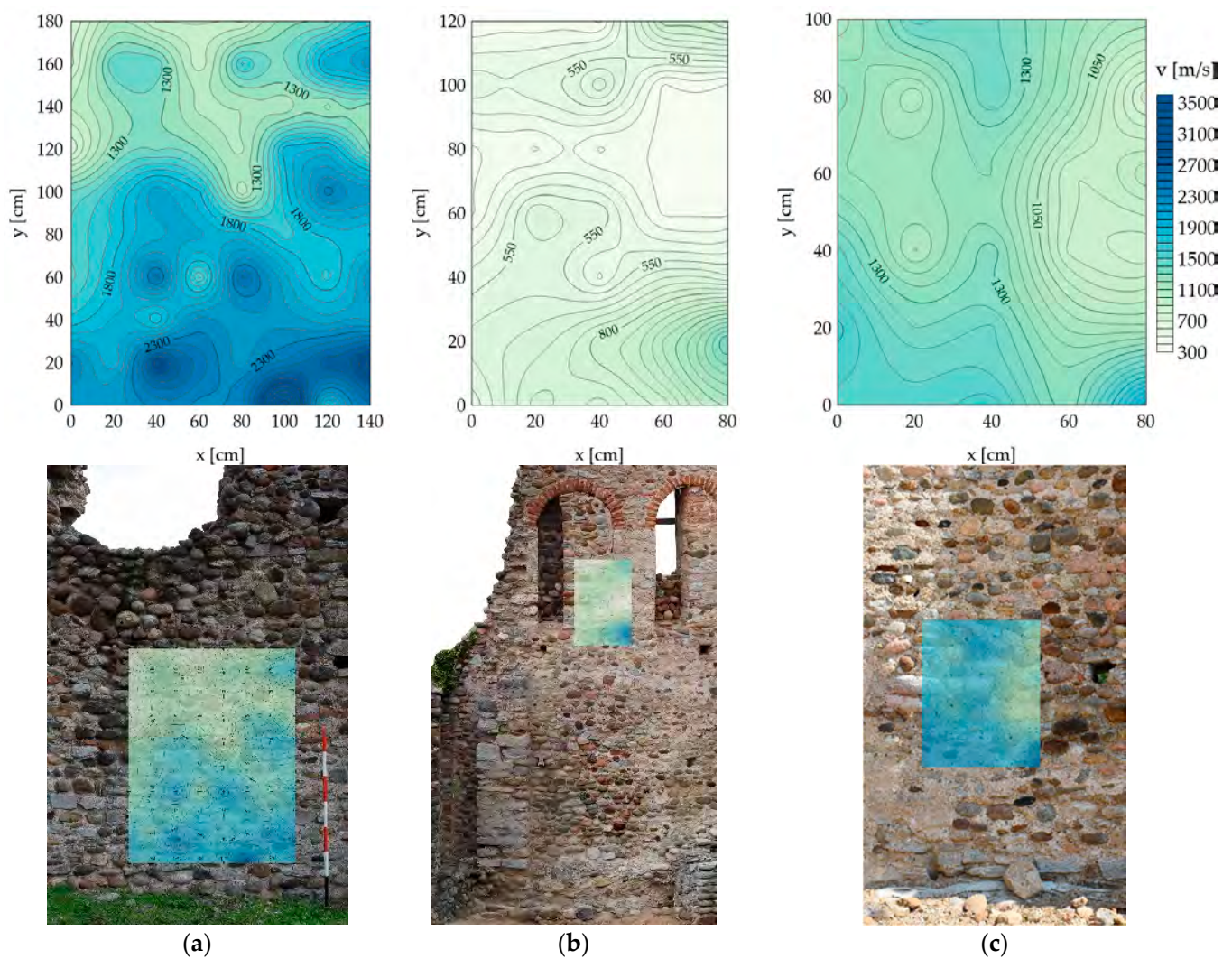


Figure 9. Sonic tests, contour maps (above), and position of the same in the walls (below): (a) SON1; (b) SON3A; (c) SON3B.

The data collected were processed in both MACEC and ARTeMIS software for cross-comparison: the north wall through the techniques pLSCF (MACEC) and SSI (ARTeMIS), and the apse through pLSCF (MACEC) and EFDD (ARTeMIS). The latter was preferred for its accuracy in determining mode shapes.

The first three structural modes were identified by the tests on the north wall (Figure 11): a first-order bending mode, a torsional mode, and a second-order horizontal bending mode. Table 4 gives the experimental frequencies of the modes and their errors, which are less than 2%, except for the third mode.

Table 4. Experimental frequencies obtained from parametric (pLSCF) and non-parametric (SSI) procedures for the three main modes of the north wall.

Frequency	pLSCF [Hz]	SSI [Hz]	ϵ [%]
f_1	4.79	4.73	1.3
f_2	5.86	5.92	0.9
f_3	8.26	7.76	6.4

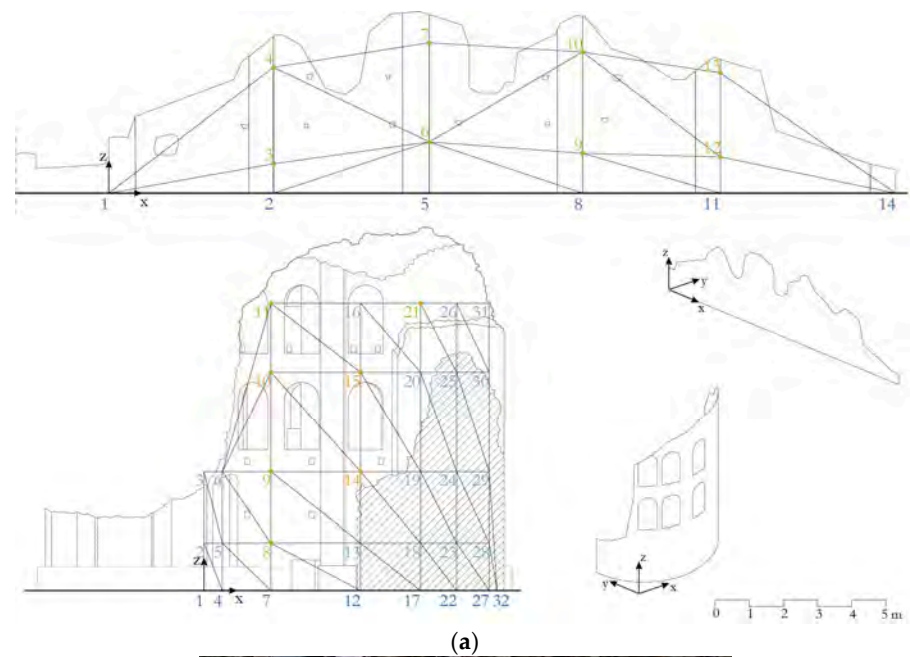


Figure 10. Setup of dynamic identification tests: (a) elevation of the grid for sensor positioning on the north wall and the apse; (b) view of accelerometers and acquisition system.

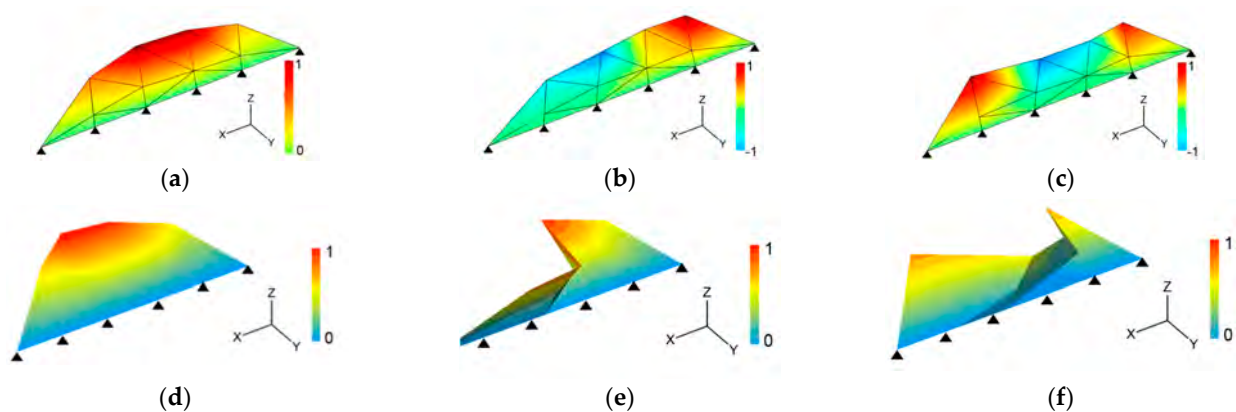


Figure 11. North wall, experimental mode shapes: (a,d) first mode; (b,e) second mode; (c,f) third mode; (a–c) processing in MACEC; (d–f) processing in ARTeMIS. The black triangles represent the fixed nodes at the base; the displacements are normalized to the maximum and minimum values.

The results of the two approaches are compared through the calculation of the MAC index (Table 5): as the indices on the diagonal of the matrix are larger than 0.9, a good consistency between the results is obtained, and thus, the calculated modes can be assumed with reasonable confidence.

Table 5. MAC indices obtained from the pLSCF and SSI procedures for the north wall.

MAC		pLSCF		
		Mode 1	Mode 2	Mode 3
SSI	Mode 1	0.991	0.043	0.046
	Mode 2	0.071	0.903	0.000
	Mode 3	0.002	0.015	0.967

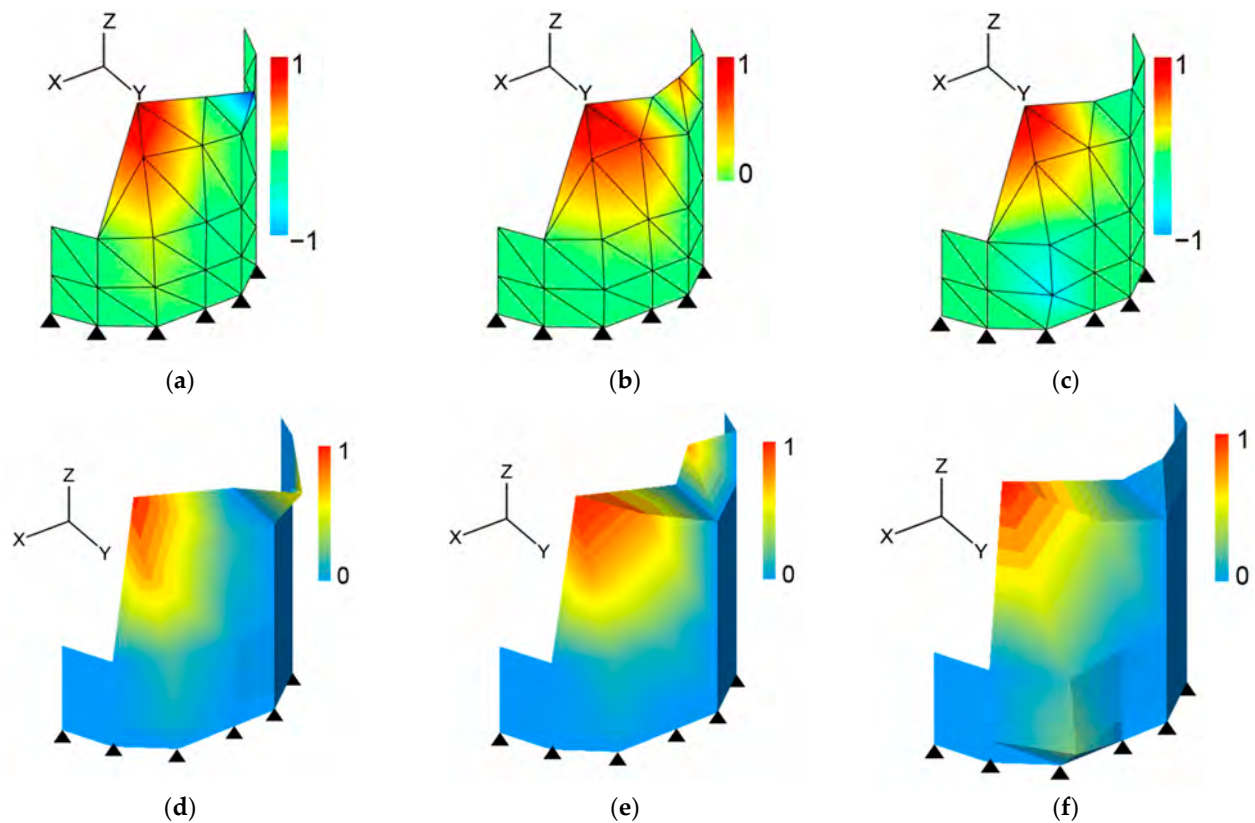
The same procedure was repeated for the apse, whose experimental frequencies and MAC indices are given in Tables 6 and 7, respectively. The first mode is torsional, the second one a first-order bending, and the third a second-order vertical bending (Figure 12).

Table 6. Experimental frequencies obtained from parametric (pLSCF) and non-parametric (EFDD) procedures for the three main modes of the apse wall.

Frequency	pLSCF (Hz)	EFDD (Hz)	ϵ (%)
f_1	4.06	4.00	1.4
f_2	4.46	4.51	1.1
f_3	5.38	5.25	2.6

Table 7. MAC indices obtained from the pLSCF and EFDD procedures for the apse wall.

MAC		pLSCF		
		Mode 1	Mode 2	Mode 3
EFDD	Mode 1	0.952	0.147	0.820
	Mode 2	0.173	0.993	0.063
	Mode 3	0.002	0.787	0.651

**Figure 12.** Main apse, experimental mode shapes: (a,d) first mode; (b,e) second mode; (c,f) third mode; (a–c) processing in MACEC; (d–f) processing in ARTeMIS. The black triangles represent the fixed nodes at the base; the displacements are normalized to the maximum and minimum values.

Despite the errors between the two procedures being less than 3%, the MAC index of the third mode is smaller than 0.9, so this mode was not properly identified through the experimental tests, and a larger number of sensors would have been required. Therefore, this mode will be discarded from the following discussion.

3.2. Structural Modeling

The shapes of the north wall and the apse were obtained from the orthophotos (Figures 4 and 5). A preliminary simplification of the walls was carried out by means of a CAD application removing niches and any irregularity of the surfaces (holes and material decay) and bordering the areas with the same thickness; the upper crest of the wall was simplified as a polyline, and the middle plane of the walls was assumed as a reference. The shapes were then imported into Strand 7 FE software (version 3.1) [84] and meshed. In total, 1910 and 1186 bidimensional 4-node or 3-node plate elements were employed in the north wall and the apse, respectively, with a maximum length of 30 cm. The base of the walls was fixed by restraining the translation of the nodes at the ground level; the strip footing of the walls was ignored in the simulation.

3.2.1. Preliminary Mechanical Properties

The mechanical properties estimated through the MQI [70] are reported in Table 8. This method obtained an interval, as prescribed by [6], which was compatible with a masonry classified as ‘two layers with internal infill’ in [6]. The north wall exhibited better construction quality, resulting in higher mechanical properties compared to the apse.

Table 8. Estimated mechanical properties from MQIs for masonry walls in S. Giovanni.

Part	f (N/mm ²)	τ_0 (N/mm ²)	E (N/mm ²)	G (N/mm ²)
North wall	1.7–2.9	0.032–0.052	906–1295	290–410
Apsse	1.2–2.1	0.019–0.031	684–984	226–320

In the FE models, in addition to the variations of thickness, the findings of the testing campaign helped in assigning a specific value within the intervals given in Table 8. The north wall (Figure 13a) was subdivided at about 1 m above the ground to take into account the results obtained from the SON1 SPVT and the MQI values from MQ9 and MQ10, which showed better construction quality in the bottom of the wall than the upper part. Therefore, the elastic moduli E of the lower part were assigned toward the maximum of the interval and oppositely for the upper one; the density value ρ was assumed preliminarily equal for all parts as that given by [6] for the compatible type (Table 9).

Table 9. Preliminary mechanical properties of the north wall (before calibration).

Area	Color (Figure 13a)	E (MPa)	ν	ρ (kg/m ³)	Thickness (m)
W1	blue	1050	0.2	2000	0.70
W2	green	950	0.2	2000	0.70
W3	red	1000	0.2	2000	1.05

The preliminary properties of the homogeneous areas of the apse are shown in Table 10. Here, MQI values (MQ7, MQ15, and MQ16) were smaller than those of the north wall, suggesting generally lower mechanical properties, and SPVTs highlighted lower sonic velocities at the top than at the bottom of the wall (compare SON3A to SON3B). An additional subdivision of the upper part was considered to account for the strengthening interventions with epoxy resins carried out in the 1990s and the infill of the windows. The elastic moduli were varied within the interval of Table 8 toward the maximum and the minimum according to the quality, except for the reinforced parts; although the masonry

type by [6] was the same as the north wall, the density was reduced to account for the lower sonic velocities. Figure 13b shows the FE model of the apse that considers all the local variations in masonry properties.

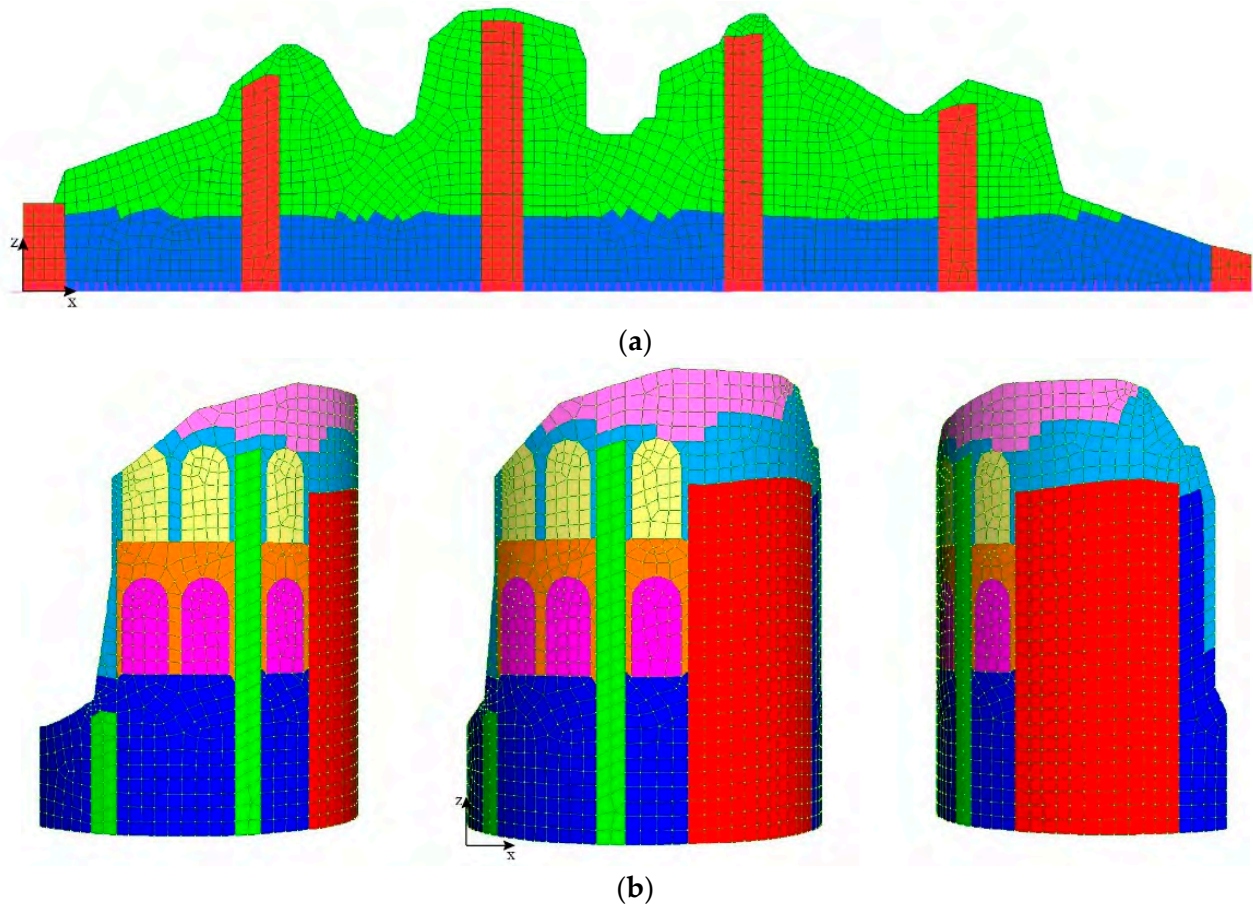


Figure 13. FE models of (a) north wall and (b) main apse. Key to colors in Tables 9 and 10, respectively.

The modal analysis on the preliminary FE model was carried out considering just the self-weight, as no variable load was applied to the walls. Table 11 reports the frequencies of the numerical modes and the relative difference ε to experimental ones obtained with both MACEC and ARTEMIS. In the north wall, numerical modal shapes match the experimental ones, and the MAC indices, ranging from 0.70 to 0.90, show a good correlation. However, the errors are too high ($\varepsilon > 10\%$), meaning that the updating of mechanical properties is required. Conversely, the apse model is already satisfactory for the first two modes ($\varepsilon < 2\%$, $\text{MAC} > 0.90$).

Table 10. Preliminary mechanical properties of the apse wall (before calibration).

Area	Color (Figure 13b)	E (MPa)	ν	ρ (kN/m ³)	Thickness (m)
A1	blue	800	0.2	1900	0.70
	green	800	0.2	1900	1.05
A2	orange	700	0.2	1700	0.70
A3	cyan	950	0.2	1800	0.70
A4	pink	950	0.2	1800	0.45
A5	red	1000	0.2	1800	0.85
A6	magenta	700	0.2	1700	0.30
A7	yellow	1100	0.2	1800	0.70

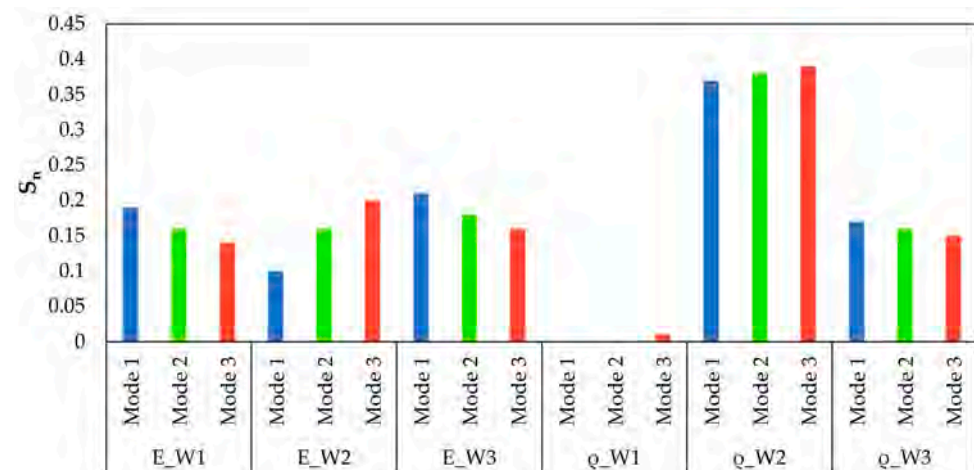
Table 11. Modal frequencies of the numerical models, errors, and MAC indices with the experimental results.

Part	Frequency	FE (Hz)	ε FE-pLSCF (%)	MAC FE-pLSCF	ε FE-SSI (%)	MAC FE-SSI	ε FE-EFDD (%)	MAC FE-EFDD
North wall	f_1	5.14	7.27	0.918	8.70	0.893	-	-
	f_2	6.80	15.93	0.793	14.84	0.870	-	-
	f_3	9.21	11.49	0.784	18.79	0.855	-	-
Apse	f_1	4.06	0.13	0.962	-	-	1.50	0.987
	f_2	4.43	0.56	0.972	-	-	1.66	0.986

3.2.2. Model Updating

A sensitivity analysis was conducted in the numerical model to verify the impact of varying the initial mechanical properties on the frequencies obtained from modal analysis. The elastic modulus E and the density ρ values were varied, while the Poisson's ratio ν remained constant. Variations of $\pm 10\%$ and $\pm 20\%$, were applied to the initial values. For each parameter, a modal analysis was performed in the FEM environment, keeping the others unchanged. The obtained frequencies were then processed using Equation (1) to obtain the sensitivity index (S_n): a higher S_n value indicates a greater impact of that property on the frequency variation in the model.

As depicted in Figure 14, the most influential parameter (S_n about 0.40) on the three modes was ρ_{W2} , i.e., the density associated with the upper portion of the wall (W2). Conversely, variations in the density of the lower portion of the wall appeared to be irrelevant for the model (W1). The elastic moduli of the three considered properties (W1–W3) and the density of the buttresses (W3) had a similar impact on the FE model, with S_n values ranging between 0.10 and 0.21. Table 12 presents the final mechanical properties of homogeneous masonry areas for the north wall.

**Figure 14.** Sensitivity indices (S_n) from the variation of elastic modulus E and density ρ in the north wall.**Table 12.** Final mechanical properties of the north wall (after calibration).

Area	E (MPa)	ΔE (%)	ρ (kN/m ³)	$\Delta \rho$ (%)
W1	800	−24	2000	0
W2	1300	37	1800	−10
W3	800	−20	2000	0

The preliminary numerical model of the apse demonstrated already good correlation with the experimental data for the first two modes of vibration. Consequently, the properties

were adjusted according to the observations derived from the calibration of the north wall (Table 13).

Table 13. Final mechanical properties of the apse wall (after calibration).

Area	E (MPa)	ΔE (%)	ρ (kg/m ³)	$\Delta \rho$ (%)
A1	750	−6	2000	5
A2	700	0	1700	0
A3	1300	37	1800	0
A4	1300	37	1800	0
A5	1000	0	1800	0
A6	700	0	1700	0
A7	1100	0	1800	0

The frequencies associated with the first three modes of the calibrated model of the north wall are 4.73 Hz, 6.49 Hz, and 9.05 Hz (Table 14), respectively, with the modal shapes remaining flexural, torsional, and second-order flexural (Figure 15). The difference in density between the lower and upper portions is maintained to consider the result of the SPVT SON1. However, it was necessary to increase the elastic modulus of the upper portion to achieve good MAC indices. These indices, on the diagonal of the FEM-pLSCF matrix, are greater than 0.8, with that associated with the first mode exceeding 0.9. Similarly, the diagonal terms of the FEM-SSI matrix are all above 0.9, and the mean errors between the frequencies of the numerical model and the experimental ones are acceptable, with values of 7.11% for FEM-pLSCF and 8.81% for FEM-SSI (Table 14).

Table 14. Modal frequencies of the updated numerical models, errors, and MAC indices with the experimental results.

Part	Frequency	FE (Hz)	ε FE-pLSCF (%)	MAC FE-pLSCF	ε FE-SSI (%)	MAC FE-SSI	ε FE-EFDD (%)	MAC FE-EFDD
North wall	f_1	4.73	1.18	0.953	0.14	0.935	-	-
	f_2	6.49	10.69	0.841	9.65	0.912	-	-
	f_3	9.05	9.47	0.844	16.64	0.914	-	-
Apsse	f_1	4.08	0.59	0.965	-	-	1.96	0.987
	f_2	4.42	1.96	0.975	-	-	2.02	0.987

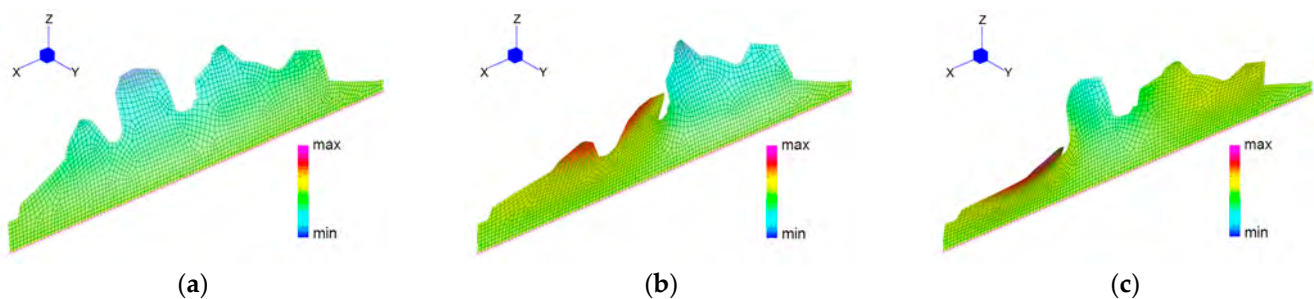


Figure 15. North wall, updated FE model mode shapes: (a) first-order bending; (b) torsional; (c) second-order bending.

The final frequencies obtained in the calibrated model of the apse are 4.08 Hz for the first mode of vibration (torsional) and 4.42 Hz for the second mode (flexural) (Figure 16), with MAC indices exceeding 0.9 for both the first two diagonal terms of the FEM-pLSCF matrix and those of the FEM-EFDD matrix (Table 14). The errors between the final frequencies obtained and the corresponding experimental analysis frequencies are negligible.

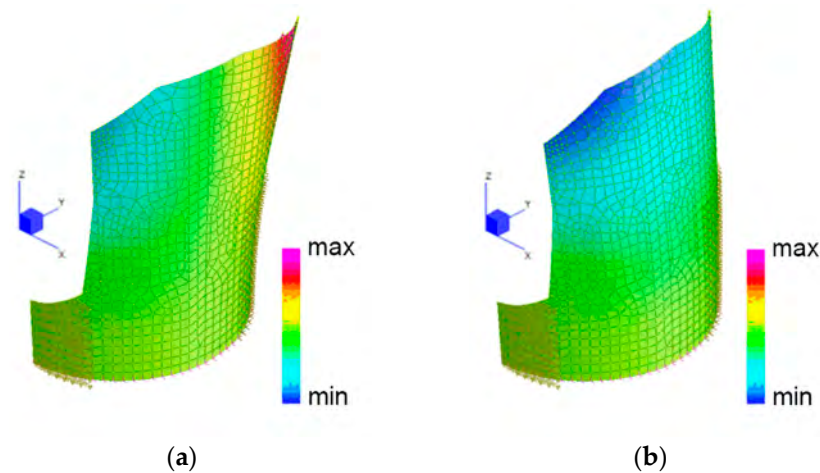


Figure 16. Apse, updated FE model mode shapes: (a) torsional; (b) bending.

3.3. Seismic Input and Safety Assessment

The base parameters of the horizontal ground spectrum prescribed by [85] for the site of S. Giovanni are shown in Table 15 for the damage limitation (DL) and no-collapse (NC) limit states (LS). The horizontal acceleration on flat bedrock (a_g) does not exceed 0.05 g at the NC limit state. The soil is almost flat, but it is made of a thick clay layer [78], which corresponds to a class D, according to [85].

Table 15. Base values for the parametric shape of the response spectrum at ground level defined by [85] for the site of S. Giovanni.

LS	a_g/g	F_0	T_C^* (s)	c_c	s_S	s_T	T_C (s)	T_B (s)	T_D (s)
DL	0.018	2.55	0.17	3.06	1.8	1	0.170	0.511	1.672
NC	0.038	2.63	0.28	2.37	1.8	1	0.220	0.660	1.752

In the MRSA, these ground spectra were applied to the restrained nodes at the base of the walls: as the out-of-plane behavior was explored, the spectra were applied perpendicularly to the mid-plane of the north wall (N–S directions) and to the diameter of the apse (E–W direction). No partial component of the spectra was considered in the perpendicular direction. The modes were combined through the SRSS combination, as the relative differences between the frequencies were larger than 10% [72].

The shear strengths of masonry were assumed as 0.040 MPa in the north wall and 0.030 MPa in the apse to account for the behavior of the mortar and the higher construction quality of the former identified in inspections and tests. Actually, the maximum allowable τ_0 according to [6] is 0.032 MPa for the most similar masonry type. The confidence factor CF was assumed as 1.35, considering the first knowledge level described by [6] as no destructive or minor-destructive tests were conducted on the structures. The resulting tensile strengths according to Equation (4) were 0.044 MPa and 0.033 MPa for the wall and the apse, respectively.

At the DL limit state, in the north wall, a cylindrical hinge formed approximately at the level of the construction joint, where a change in mechanical properties was detected through the tests (Figure 17a, compare Figure 13a). At the NC limit state, due to higher forces, the tensile strength is reached at a higher level, in the areas corresponding to the three wall ridges (Figure 17b).

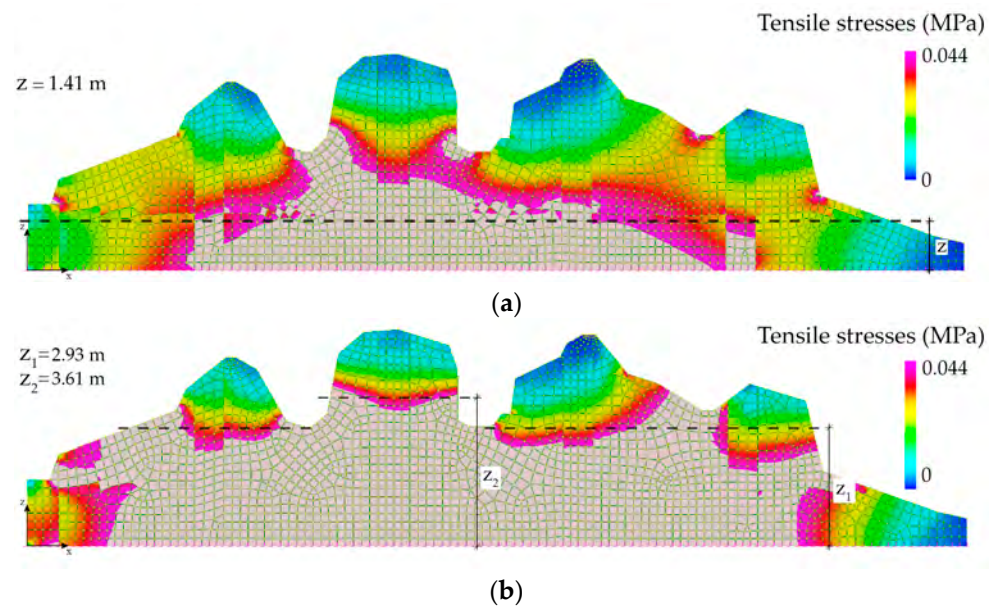


Figure 17. Combined tensile stresses in the north wall at: (a) DL; (b) NC limit states. Stresses are capped at the tensile strength (blank part), and hinge positions are highlighted by the dashed lines.

In the main apse, the lateral portions of the structure exceeded the tensile strength at the DL limit state, identifying two wedge-shaped macroblocks. At the NC limit state, four possible hinges were identified: one corresponding to the lateral portions, two to diagonal portions of the wall with hinges at different levels, and one to a horizontal hinge at the level of the second-order windows, considering the weakening caused by the localized narrowing of the masonry section (Figure 18, compare with Figure 13b).

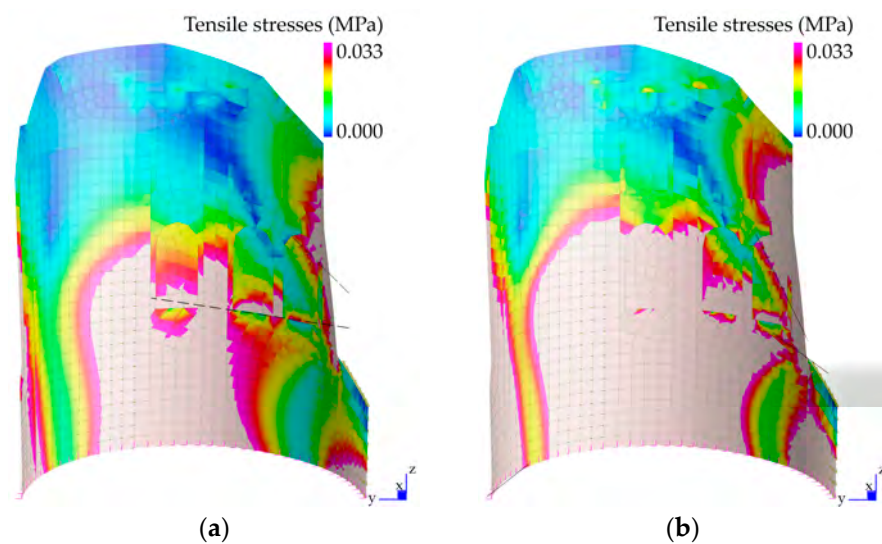


Figure 18. Combined tensile stresses in the apse at: (a) DL; (b) NC limit states. Stresses are capped at the tensile strength (blank part), and hinge positions are highlighted by the dashed lines.

The macroblocks that were defined according to the positions of the hinges at the two limit states and the local mechanisms that could affect them are displayed in Figures 19 and 20 for the north wall and the apse, respectively.

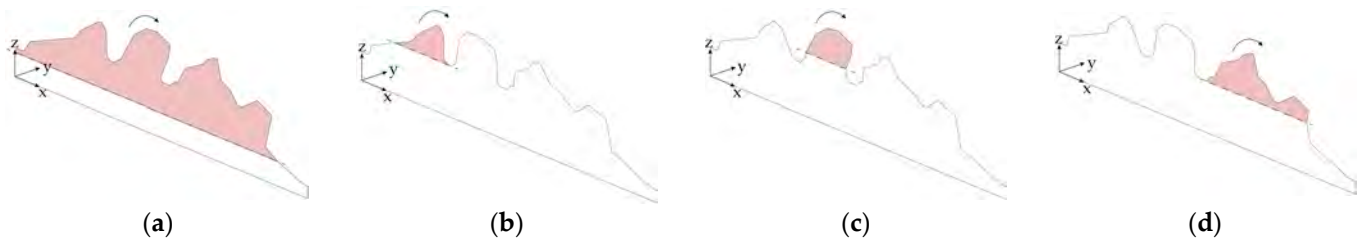


Figure 19. North wall, macroblocks, and local mechanisms of collapse (compare Figure 17): (a) DL limit state; (b–d) NC limit state.

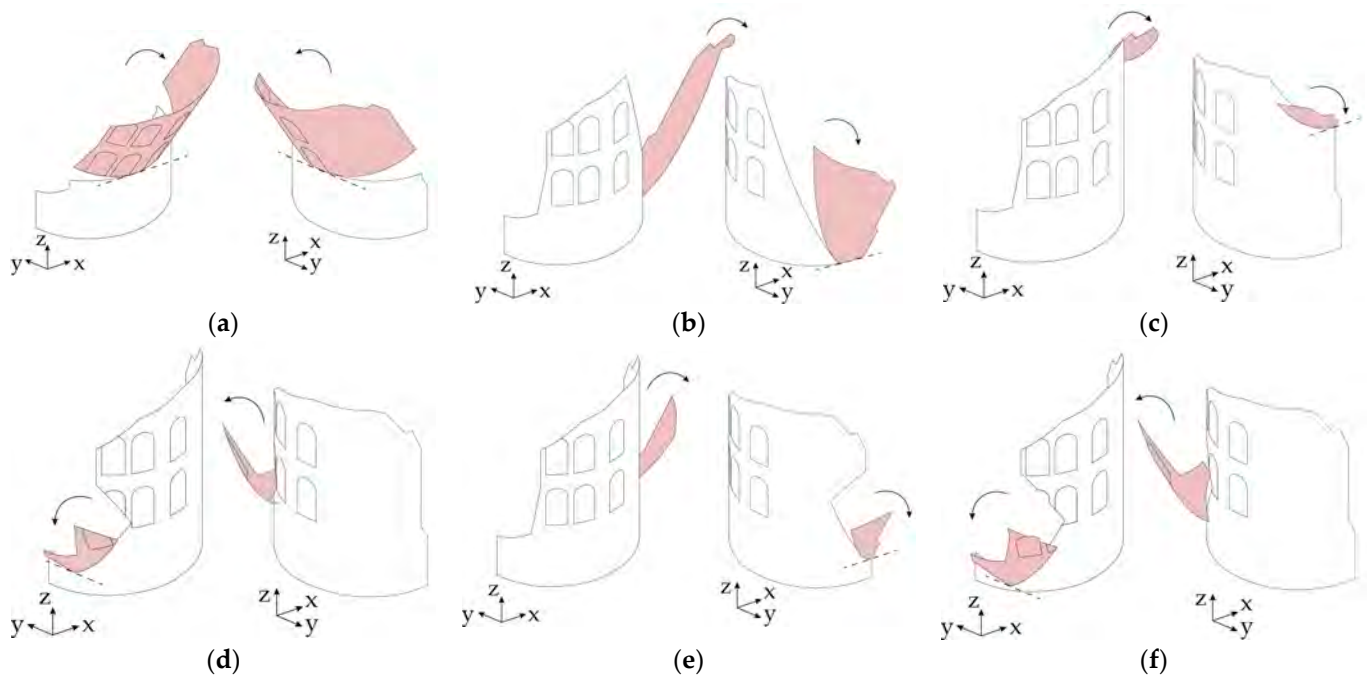


Figure 20. Apse, macroblocks, and local mechanisms of collapse (compare Figure 18): (a,b) DL limit state; (c–f) NC limit state.

Once the geometry of a macroblock is known, the value of the static multiplier λ is the ratio between its thickness and the height of its centroid, which can be determined with CAD software; then, the spectral acceleration a_0^* of the mechanism is obtained through Equation (6). The demand acceleration a_z was obtained by querying the model where the plastic hinge was detected in the SRSS combination of the modes for the two limit states. The modal frequencies of the apse did not fall inside the plateau of the ground spectrum, and therefore, the dynamic amplification was not so relevant. At the NC limit state, the demand accelerations are divided by $q = 1.5$ due to the very small energy dissipation that free-standing walls can express.

Tables 16 and 17 report the relevant capacity (a_0^*) and demand (a_z) accelerations at the two reference limit states and the outcome of the safety assessment for the possible mechanisms in the north wall and the apse, respectively. In spite of the dynamic amplification, the mechanisms did not activate as the demand was always smaller than the capacity, with a safety ratio (capacity vs. demand, i.e., a_0^*/a_z) that was on average 4.96 for the north wall and 3.20 for the apse (NC limit state). It is worth noting that some of the detected mechanisms in the apse had the plastic hinge very close to the ground level, so the acceleration demand did not differ much from the ground motion.

Table 16. Safety assessment of the local mechanisms in the north wall (see Figure 19).

Mechanism	Limit State	λ	a_0^* (m/s ²)	a_z (m/s ²)	Safety Ratio	Activation
1 (Figure 19a)	DL	0.25	1.82	0.30	6.06	No
2 (Figure 19b)	NC	0.56	4.06	1.35	3.01	No
3 (Figure 19c)	NC	0.47	3.41	1.11	3.07	No
4 (Figure 19d)	NC	0.50	3.63	1.35	2.68	No

Table 17. Safety assessment of the local mechanisms in the apse (see Figure 20).

Mechanism	Limit State	λ	a_0^* (m/s ²)	a_z (m/s ²)	Safety Ratio	Activation
1 (Figure 20a)	DL	0.12	0.87	0.32	2.71	No
2 (Figure 20b)	DL	0.76	5.52	1.21	4.56	No
3 (Figure 20c)	NC	0.29	2.11	0.38	5.55	No
4 (Figure 20d)	NC	0.15	1.09	0.44	2.47	No
5 (Figure 20e)	NC	0.14	1.01	0.39	2.58	No
6 (Figure 20f)	NC	0.12	0.87	0.40	2.18	No

4. Discussion

The texture and the mortar of the apse are moderately different from the north wall, since smaller elements were employed, and crushed pottery instead of clay was used for inducing a pozzolanic reaction. This may be a result of different construction practices, but more information can come from specific studies on the mortars, which are now limited to that used in the tombs [81].

The MQI method is calibrated on medieval and modern masonry systems, which can be categorized according to the standards outlined in [6], but the specific type of masonry used in S. Giovanni does not fit neatly within these predefined categorizations, being more ancient. However, the main incompatibility between the method and the actual masonry resides in the mortar and its internal composition, whose good quality compensated for the poor texture. ENDS and SPVTs helped in confirming the hypothesis of good masonry, although they pointed out some differences between the north wall and the apse. Indeed, the sonic velocities obtained in this study are much higher than those observed in ancient Pompeii [47], except for SON3A, and they are comparable to the results of [26], who studied a Roman concrete structure. The sonic velocity of the apse was lower than that of the north wall (about 500 m/s), probably as a consequence of a longer exposition to the weathering effects; in general, the sonic velocities were higher in the lower parts of the structures, which had been covered by the ground until recent times [78]. It is strange that a soft stone was used for the pillars of the windows in the apse, but probably, the need to cut it into small blocks that could fit the regular shape of this element prevailed over strength considerations.

The results of the dynamic identification are compatible with previous studies (e.g., [13]) and confirm that the main response of such structures is governed by an out-of-plane response, although just the first mode is the most relevant. However, an additional study is required on the apse.

The dimension of the macroblocks reduces as the ground motion increases, passing from the DL to the NC limit states, since the tensile strength is reached earlier in the material. This variability may be interpreted as upper and lower bounds in the shape of the elements, although a more refined evaluation can be obtained by introducing the uncertainty in the strength of the material. However, a cross-comparison of these observations would require nonlinear dynamic analyses. The static multipliers are quite high for simple overturning, due to the thickness of the walls, and the safety ratios largely exceed 1 (total safety) due to the low seismic input expected for the site. However, the safety ratios reduce passing from the DL to the NC limit states (from about 4 to about 2) as a consequence of the larger input; the minimum value is 2.20 for a mechanism in the apse. The apse generally obtained smaller safety ratios (a 2.47 average at NC) than the north wall (a 2.97 average at NC) mainly due to its smaller tensile strength, which determined larger macroblocks. Indeed,

the dynamic amplification is smaller in the apse than in the north wall, as the period of the modes falls outside the plateau of the ground spectra.

5. Conclusions

This study focuses on the structural investigations and safety assessment of S. Giovanni, the primary church in Castelseprio, an early medieval settlement in northern Italy. Currently, only the north wall and the main apse of this site stand prominently, with the settlement having been abandoned in the late 13th century.

The exploratory study carried out preliminarily to the safety assessment confirms the need of approaching various testing procedures and cross-checking the results of each to obtain reliable information about the status of heritage structures. The dynamic identification was an important step of the exploratory study as it allowed the final calibration of the mechanical properties of the materials, which could not be directly determined from non-destructive tests.

The safety assessment is grounded in the criteria of the limit analysis, although a refinement of the conventional rigid-block approach is proposed by considering the results of a modal response spectrum analysis on the calibrated model to determine the shape and the position of the macroblocks. This approach is simple yet up to date in respect to recent studies on heritage structures and can be easily implemented by professionals and researchers in other sites, thus offering a valuable tool for their management. However, two main limitations may be detected in the proposed method and can guide further studies. First, a cross-comparison of the shape of the macroblocks can be obtained by means of nonlinear dynamic analyses on discrete or continuous models. Second, the identification of the macroblocks depends on the value of the tensile strength, which was determined from an indirect evaluation (i.e., the masonry quality index). Therefore, a probabilistic approach, considering upper and lower bounds for this parameter, would account for this uncertainty by obtaining a distribution of accelerations of activation from which fragility curves can be obtained.

Author Contributions: Conceptualization, L.S., A.C.A., G.P.B. and M.R.V.; methodology, L.S. and L.T.; software, L.T. and A.C.; validation, L.S., L.T., Y.S. and A.C.; formal analysis, L.S., L.T. and A.C.; investigation, L.S., L.T., Y.S., A.C., A.C.A. and G.P.B.; resources, M.R.V.; data curation L.S., L.T., Y.S. and A.C.; writing—original draft preparation, L.S. and L.T.; writing—review and editing, L.S., Y.S. and M.R.V.; visualization, L.S. and L.T.; supervision, A.C.A., G.P.B. and M.R.V.; project administration, A.C.A. and G.P.B.; funding acquisition, M.R.V. All authors have read and agreed to the published version of the manuscript.

Funding: This research received no external funding.

Data Availability Statement: The data obtained from sonic pulse velocity tests are available upon request to the corresponding author.

Acknowledgments: The authors wish to thank the Soprintendenza Archeologia, Belle Arti e Paesaggio per le province di Como, Lecco, Monza-Brianza, Pavia, Sondrio e Varese, the Parco Archeologico e Antiquarium di Castelseprio, and the Direzione regionale Musei Lombardia for providing access to the site and allowing the tests.

Conflicts of Interest: The authors declare no conflicts of interest.

References

1. Cecchi, R.; Gasparoli, P. *Prevenzione e Manutenzione per i Beni Culturali Edificati*; Alinea: Florence, Italy, 2010.
2. *Archaeological Sites: Conservation and Management*; Sullivan, S.; Mackay, R. (Eds.) Readings in Conservation; The Getty Conservation Institute: Los Angeles, CA, USA, 2012; ISBN 978-1-60606-124-4.
3. Teutonico, J.M.; Palumbo, G. (Eds.) *Management Planning for Archaeological Site*; The Getty Conservation Institute: Los Angeles, CA, USA, 2002.
4. Giuffré, A. A Mechanical Model for Statics and Dynamics of Historical Masonry Buildings. In *Protection of the Architectural Heritage Against Earthquakes*; Petrini, V., Save, M., Eds.; Springer Vienna: Vienna, Austria, 1996; pp. 71–152, ISBN 978-3-211-82805-2.

5. ICOMOS-ISCARSAH Committee. Recommendations for the Analysis, Conservation and Structural Restoration of Architectural Heritage. 2003. Available online: https://ancientgeorgia.files.wordpress.com/2012/04/recommendations_icomos-principles-and-guidelines.pdf (accessed on 12 January 2024).
6. Ministry of Infrastructures and Transportations. Regulation No. 7/2019, Istruzioni per L'applicazione dell'«Aggiornamento Delle “Norme Tecniche per Le Costruzioni”» di cui al Decreto Ministeriale 17 Gennaio 2018. 2019. Available online: <https://www.gazzettaufficiale.it/eli/id/2019/02/11/19A00855/sg> (accessed on 12 January 2024). (In Italian)
7. Bosiljkov, V.; Uranjek, M.; Žarnić, R.; Bokan-Bosiljkov, V. An Integrated Diagnostic Approach for the Assessment of Historic Masonry Structures. *J. Cult. Herit.* **2010**, *11*, 239–249. [[CrossRef](#)]
8. Marino, L. *Conservazione e Manutenzione di Manufatti Edilizi Ridotti allo Stato di Rudere*; Opus Libri: Florence, Italy, 1989.
9. Baggio, C. La Valutazione Della Sicurezza (Strutturale): Analitica o Qualitativa. In *Quale Sicurezza per il Patrimonio Architettonico?* Centroni, A., Ed.; Nuova Argos: Roma, Italy, 2007; pp. 133–142. (In Italian)
10. Lourenço, P.B.; Mendes, N.; Ramos, L.F.; Oliveira, D.V. Analysis of Masonry Structures without Box Behavior. *Int. J. Archit. Herit.* **2011**, *5*, 369–382. [[CrossRef](#)]
11. Degli Abbati, S.; Cattari, S.; Lagomarsino, S. Theoretically-Based and Practice-Oriented Formulations for the Floor Spectra Evaluation. *Earthq. Struct.* **2018**, *15*, 565–581. [[CrossRef](#)]
12. Degli Abbati, S.; D’Altri, A.M.; Ottonelli, D.; Castellazzi, G.; Cattari, S.; de Miranda, S.; Lagomarsino, S. Seismic Assessment of Interacting Structural Units in Complex Historic Masonry Constructions by Nonlinear Static Analyses. *Comput. Struct.* **2019**, *213*, 51–71. [[CrossRef](#)]
13. Aguilar, R.; Marques, R.; Sovero, K.; Martel, C.; Trujillano, F.; Boroschek, R. Investigations on the Structural Behaviour of Archaeological Heritage in Peru: From Survey to Seismic Assessment. *Eng. Struct.* **2015**, *95*, 94–111. [[CrossRef](#)]
14. Di Miceli, E.; Monti, G.; Bianco, V.; Filetici, M.G. Assessment and Improvement of the Seismic Safety of the “Bastione Farnesiano”, in the Central Archeological Area of Rome: A Calculation Method between Need to Preserve and Uncertainties. *Int. J. Archit. Herit.* **2017**, *11*, 198–218. [[CrossRef](#)]
15. Bergamasco, I.; Papaccio, V.; Carpani, B.; Clemente, P.; Saitta, F. Seismic Preservation of the Archeological Site of Pompeii. Preliminary Analyses. *Energ. Ambiente Innov.* **2012**, *2*, 48–55.
16. Galassi, S.; Ruggieri, N.; Tempesta, G. A Novel Numerical Tool for Seismic Vulnerability Analysis of Ruins in Archaeological Sites. *Int. J. Archit. Herit.* **2020**, *14*, 1492647. [[CrossRef](#)]
17. Pappas, A.; Da Porto, F.; Modena, C. Seismic Vulnerability Assessment Form for Free-Standing Columns Based on a Simplified Numerical Analysis. *Int. J. Archit. Herit.* **2016**, *10*, 281–299. [[CrossRef](#)]
18. Valluzzi, M.R.; Salvalaggio, M.; Lorenzoni, F.; Politi, M.; Boaga, J. The Engineering Approach to Conservation of Massive Archaeological Structures in Seismic Areas: The Apollo Nymphaeum in Hierapolis of Phrygia. *Int. J. Archit. Herit.* **2023**, *17*, 1590–1606. [[CrossRef](#)]
19. Pulatsu, B.; Bretas, E.M.; Lourenco, P.B. Discrete Element Modeling of Masonry Structures: Validation and Application. *Earthq. Struct.* **2016**, *11*, 563–582. [[CrossRef](#)]
20. Doherty, K.; Griffith, M.C.; Lam, N.; Wilson, J. Displacement-Based Seismic Analysis for out-of-Plane Bending of Unreinforced Masonry Walls. *Earthq. Eng. Struct. Dyn.* **2002**, *31*, 833–850. [[CrossRef](#)]
21. Heyman, J. *The Stone Skeleton: Structural Engineering of Masonry Architecture*; Cambridge University Press: New York, NY, USA, 1997; ISBN 978-0-521-62963-8.
22. D’Ayala, D.; Speranza, E. Definition of Collapse Mechanisms and Seismic Vulnerability of Historic Masonry Buildings. *Earthq. Spectra* **2003**, *19*, 479–509. [[CrossRef](#)]
23. Kouris, L.A.S.; Penna, A.; Magenes, G. Seismic Damage Diagnosis of a Masonry Building Using Short-Term Damping Measurements. *J. Sound Vib.* **2017**, *394*, 366–391. [[CrossRef](#)]
24. Ferretti, D.; Coisson, E.; Lenticchia, E. Seismic Damage on Merlons in Masonry Fortified Buildings: A Parametric Analysis for Overturning Mechanism. *Eng. Struct.* **2018**, *177*, 117–132. [[CrossRef](#)]
25. Roca, P. The ISCARSAH Guidelines on the Analysis, Conservation and Structural Restoration of Architectural Heritage. In Proceedings of the 12th International Conference on Structural Analysis of Historical Constructions (SAHC), Barcelona, Spain, 16–18 September 2020; Roca, P., Pelà, L., Molins, C., Eds.; International Centre for Numerical Methods in Engineering (CIMNE): Barcelona, Spain, 2021; pp. 1629–1640.
26. Guerriero, L.; Guadagnuolo, M.; Titomanlio, I.; Faella, G. An Integrated Approach for the Conservation of Archaeological Buildings: The “Re Barbaro” Palace in Sardinia. *Digit. Appl. Archaeol. Cult. Herit.* **2022**, *27*, e00244. [[CrossRef](#)]
27. Valluzzi, M.R.; Lorenzoni, F.; Deiana, R.; Taffarel, S.; Modena, C. Non-Destructive Investigations for Structural Qualification of the Sarno Baths, Pompeii. *J. Cult. Herit.* **2019**, *40*, 280–287. [[CrossRef](#)]
28. Marques, R.; Aguilar, R.; Trujillano, F.; Sovero, K.; Martel, C. Study on the Seismic Behaviour of Archaeological Heritage Buildings: A Wall in Chokepukio. In Proceedings of the 9th International Conference on Structural Analysis of Historical Constructions (SAHC), Mexico City, Mexico, 14–17 October 2014.
29. Lanzarone, F. *La Conservazione Dei Beni Culturali. Processo Conservativo e Vigente Normativa, Il Nuovo Codice Urbani*; Flaccovio: Palermo, Italy, 2004. (In Italian)
30. Angjeliu, G.; Coronelli, D.; Cardani, G. Development of the Simulation Model for Digital Twin Applications in Historical Masonry Buildings: The Integration between Numerical and Experimental Reality. *Comput. Struct.* **2020**, *238*, 106282. [[CrossRef](#)]

31. Dal Piaz, V. Il Ruolo Delle Fonti Documentarie: Appunti Di Metodo. In *Manutenzione e Conservazione del Costruito fra Tradizione e Innovazione: Atti del Convegno di Studi "Scienza e Beni Culturali"*, Bressanone 24-27 Giugno 1986; Biscontin, G., Ed.; Libreria Progetto: Padova, Italy, 1986; pp. 1–9. (In Italian)
32. Stylianidis, E.; Remondino, F. (Eds.) *3D Recording, Documentation and Management of Cultural Heritage*; Whittles Publishing: Dunbeath, UK, 2016.
33. Castillo, L.J.; Serván, F.; Patroni, K. Documenting Archaeological Sites on Mountains and Slopes with Drones. *Adv. Archaeol. Pract.* **2019**, *7*, 337–352. [[CrossRef](#)]
34. Mannoni, T. *Caratteri Costruttivi dell'Edilizia Storica*; Venticinque Anni di Archeologia Globale; ESCUM: Genova, Italy, 1994.
35. Boato, A. *L'archeologia in Architettura. Misurazioni, Stratigrafie, Datazioni, Restauro*; Marsilio: Venice, Italy, 2008.
36. Borri, A.; Corradi, M.; Castori, G.; De Maria, A. A Method for the Analysis and Classification of Historic Masonry. *Bull. Earthq. Eng.* **2015**, *13*, 2647–2665. [[CrossRef](#)]
37. Doglioni, F. Processi Di Trasformazione e Forme Di Vulnerabilità. In *Tecniche Costruttive dell'Edilizia Storica. Conoscere per Conservare*; Fiorani, D., Esposito, D., Eds.; Viella: Roma, Italy, 2005; pp. 219–231.
38. Cardani, G.; Binda, L. Guidelines for the Masonry Quality Evaluation in Built Heritage. In *Proceedings of the International Conference Built Heritage 2013: Monitoring Conservation Management*, Milan, Italy, 18–20 November 2013; pp. 107–115.
39. Rovero, L.; Alecci, V.; Mechelli, J.; Tonietti, U.; De Stefano, M. Masonry Walls with Irregular Texture of L'Aquila (Italy) Seismic Area: Validation of a Method for the Evaluation of Masonry Quality. *Mater. Struct.* **2016**, *49*, 2297–2314. [[CrossRef](#)]
40. Manzo, A.; Cantini, L.; Chesi, C.; Parisi, M.A. Italian Middle Byzantine Churches: A Comparison Through Masonry Quality Analysis. *Int. J. Archit. Herit.* **2021**, *15*, 1474–1491. [[CrossRef](#)]
41. Borri, A.; Corradi, M.; De Maria, A. The Failure of Masonry Walls by Disaggregation and the Masonry Quality Index. *Heritage* **2020**, *3*, 1162–1198. [[CrossRef](#)]
42. Borri, A.; De Maria, A. Il Metodo IQM per la Stima delle Caratteristiche Meccaniche delle Murature: Allineamento alla Circolare n. 7/2019. In *Atti del XVIII Convegno ANIDIS L'Ingegneria Sismica in Italia: Ascoli Piceno, 15–19 Settembre 2019*; Braga, F., Dall'Asta, A., Gara, F., Eds.; Pisa University Press: Pisa, Italy, 2019; pp. SG06-02–SG06-21. (In Italian)
43. Binda, L. The Importance of Investigation for the Diagnosis of Historic Buildings: Application at Different Scales (Centres and Single Buildings). In *Structural Analysis of Historical Constructions: Proceedings of the IVth. Int. Seminar on Structural Analysis of Historical Constructions, 10–13 November 2004, Padova, Italy*; Modena, C., Lourenço, P.B., Roca, P., Eds.; Taylor & Francis Group: Abingdon, UK, 2005; pp. 29–42.
44. Binda, L.; Saisi, A.; Tiraboschi, C. Investigation Procedures for the Diagnosis of Historic Masonries. *Constr. Build. Mater.* **2000**, *14*, 199–233. [[CrossRef](#)]
45. Valluzzi, M.R.; Cescatti, E.; Cardani, G.; Cantini, L.; Zanzi, L.; Colla, C.; Casarin, F. Calibration of Sonic Pulse Velocity Tests for Detection of Variable Conditions in Masonry Walls. *Constr. Build. Mater.* **2018**, *192*, 272–286. [[CrossRef](#)]
46. Autiero, F.; De Martino, G.; Di Ludovico, M.; Prota, A. Mechanical Performance of Full-Scale Pompeii-like Masonry Panels. *Constr. Build. Mater.* **2020**, *251*, 118964–118979. [[CrossRef](#)]
47. Autiero, F.; De Martino, G.; Di Ludovico, M.; Prota, A. Structural Assessment of Ancient Masonry Structures: An Experimental Investigation on Rubble Stone Masonry. *Int. J. Archit. Herit.* **2023**, *17*, 815–828. [[CrossRef](#)]
48. Miranda, L.; Cantini, L.; Guedes, J.; Binda, L.; Costa, A. Applications of Sonic Tests to Masonry Elements: Influence of Joints on the Propagation Velocity of Elastic Waves. *J. Mater. Civ. Eng.* **2013**, *25*, 667–682. [[CrossRef](#)]
49. Saretta, Y.; Casarin, F.; Valluzzi, M.R. An Update of Sonic Pulse Velocity Tests on Heritage Buildings: Correlation with Masonry Types. In *Structural Analysis of Historical Constructions*; Endo, Y., Hanazato, T., Eds.; RILEM Bookseries; Springer Nature Switzerland: Cham, Switzerland, 2024; Volume 47, pp. 654–667, ISBN 978-3-031-39602-1.
50. Rainieri, C.; Fabbrocino, G. Operational Modal Analysis for the Characterization of Heritage Structures. *Geofizika* **2011**, *28*, 109–126.
51. Malcata, M.; Ponte, M.; Tiberti, S.; Bento, R.; Milani, G. Failure Analysis of a Portuguese Cultural Heritage Masterpiece: Bonet Building in Sintra. *Eng. Fail. Anal.* **2020**, *115*, 104636. [[CrossRef](#)]
52. Requena-Garcia-Cruz, M.V.; Romero-Sánchez, E.; López-Piña, M.P.; Morales-Esteban, A. Preliminary Structural and Seismic Performance Assessment of the Mosque-Cathedral of Cordoba: The Abd al-Rahman I Sector. *Eng. Struct.* **2023**, *291*, 116465. [[CrossRef](#)]
53. Shabani, A.; Kioumars, M.; Zucconi, M. State of the Art of Simplified Analytical Methods for Seismic Vulnerability Assessment of Unreinforced Masonry Buildings. *Eng. Struct.* **2021**, *239*, 112280. [[CrossRef](#)]
54. Lorenzoni, F.; Casarin, F.; Modena, C.; Caldon, M.; Islami, K.; da Porto, F. Structural Health Monitoring of the Roman Arena of Verona, Italy. *J. Civ. Struct. Health Monit.* **2013**, *3*, 227–246. [[CrossRef](#)]
55. Chácará, C.; Zvietcovich, F.; Briceño, C.; Marques, R.; Perucchio, R.; Castañeda, B.; Uceda, S.; Morales, R.; Aguilar, R. On-Site Investigation and Numerical Analysis for Structural Assessment of the Archaeological Complex of Huaca de La Luna. In *Proceedings of the 9th International Conference on Structural Analysis of Historical Constructions*, Mexico City, Mexico, 14–17 October 2014.
56. Brincker, R.; Zhang, L.; Andersen, P. Modal Identification from Ambient Response Using Frequency Domain Decomposition. In *Proceedings of the SEM Annual Conference and Exposition on Experimental and Applied Mechanics*, San Antonio, TX, USA, 14–17 September 2000.

57. Guillaume, P.; Verboven, P.; Vanlanduit, S.; Van der Auweraer, H.; Peeters, B. A Poly-Reference Implementation of the Least-Squares Complex Frequency-Domain Estimator. In Proceedings of the SEM Annual Conference and Exposition on Experimental and Applied Mechanics, Kissimmee, FL, USA, 3–6 February 2003.
58. Peeters, B.; De Roeck, G. Stochastic System Identification for Operational Modal Analysis: A Review. *J. Dyn. Syst. Meas. Control* **2001**, *123*, 659–667. [[CrossRef](#)]
59. *ARTEMIS Extractor*; Release 6.0 2011; Structural Vibration Solutions A/S SVS: Aalborg, Denmark, 2011.
60. Van den Branden, B.; Laquière, A.; Peeters, B.; De Roeck, G. *MACEC 2021, Version 3.4*; KU Leuven: Leuven, Belgium, 2021.
61. Lourenço, P.B.; Gaetani, A. *Finite Element Analysis for Building Assessment: Advanced Use and Practical Recommendations*, 1st ed.; Routledge: New York, NY, USA, 2022; ISBN 978-0-429-34156-4.
62. Ghiassi, B.; Milani, G. (Eds.) *Numerical Modelling of Masonry and Historical Structures: From Theory to Application*; Woodhead Publishing Series in Civil and Structural Engineering; Woodhead Publishing: Duxford, UK, 2019; ISBN 978-0-08-102439-3.
63. D’Altri, A.M.; Sarhosis, V.; Milani, G.; Rots, J.; Cattari, S.; Lagomarsino, S.; Sacco, E.; Tralli, A.; Castellazzi, G.; de Miranda, S. Modeling Strategies for the Computational Analysis of Unreinforced Masonry Structures: Review and Classification. *Arch. Comput. Methods Eng.* **2020**, *27*, 1153–1185. [[CrossRef](#)]
64. Sánchez-Aparicio, L.J.; Riveiro, B.; González-Aguilera, D.; Ramos, L.F. The Combination of Geomatic Approaches and Operational Modal Analysis to Improve Calibration of Finite Element Models: A Case of Study in Saint Torcato Church (Guimarães, Portugal). *Constr. Build. Mater.* **2014**, *70*, 118–129. [[CrossRef](#)]
65. Elyamani, A.; Roca, P. A Review on the Study of Historical Structures Using Integrated Investigation Activities for Seismic Safety Assessment. Part II: Model Updating And Seismic Analysis. *Sci. Cult.* **2018**, *4*, 29–51. [[CrossRef](#)]
66. Cattari, S.; Degli Abbatì, S.; Alfano, S.; Brunelli, A.; Lorenzoni, F.; da Porto, F. Dynamic Calibration and Seismic Validation of Numerical Models of URM Buildings through Permanent Monitoring Data. *Earthq. Eng. Struct. Dyn.* **2021**, *50*, 2690–2711. [[CrossRef](#)]
67. Beconcini, M.L.; Croce, P.; Mengozzi, M. Dynamic Monitoring and Model Updating of a Masonry Bell Tower in Pisa. In Proceedings of the 5th International Conference on Structural Analysis of Historical Constructions, New Delhi, India, 6–8 November 2006; Lourenço, P.B., Roca, P., Modena, C., Agrawal, S., Eds.; Macmillan: New Delhi, India, 2007; pp. 659–666.
68. Gentile, C.; Saisi, A. Ambient Vibration Testing of Historic Masonry Towers for Structural Identification and Damage Assessment. *Constr. Build. Mater.* **2007**, *21*, 1311–1321. [[CrossRef](#)]
69. Gentile, C.; Saisi, A.; Gallino, N. Operational Modal Analysis and FE Modelling of a Masonry Tower. In Proceedings of the 3rd International Operational Modal Analysis Conference (IOMAC), Portonovo, Italy, 4–6 May 2009; pp. 499–506.
70. Allemang, R.J.; Brown, D.L. A Correlation Coefficient for Modal Vector Analysis. In Proceedings of the 1st International Modal Analysis Conference, Orlando, FL, USA, 8–10 November 1982; pp. 110–116.
71. Pastor, M.; Binda, M.; Harčarik, T. Modal Assurance Criterion. *Model. Mech. Mechatron. Syst.* **2012**, *48*, 543–548. [[CrossRef](#)]
72. European Committee for Standardization. Eurocode 8: Design of Structures for Earthquake Resistance—Part 1: General Rules, Seismic Actions and Rules for Buildings (EN 1998-1: 2004). 2004. Available online: <https://www.confinedmasonry.org/wp-content/uploads/2009/09/Eurocode-8-1-Earthquakes-general.pdf> (accessed on 12 January 2004).
73. Turnšek, V.; Čačovič, F. Some Experimental Results on the Strength of Brick Masonry Walls. In Proceedings of the 2nd International Brick Masonry Conference, Stoke-on-Trent, UK, 12–15 April 1970; pp. 149–156.
74. Donà, M.; Carpanese, P.; Follador, V.; Sbrogiò, L.; da Porto, F. Mechanics-Based Fragility Curves for Italian Residential URM Buildings. *Bull. Earthq. Eng.* **2021**, *19*, 3099–3127. [[CrossRef](#)]
75. Chavarria Arnau, A.; Brogiolo, G.P.; Vedovetto, P. Nuove Indagini Sulla Chiesa Di San Giovanni Di Castelseprio (VA). Campagne Di Scavo 2021. In *IX Congresso Nazionale di Archeologia Medievale, Alghero, 28 Settembre–2 Ottobre 2022*; Milanese, M., Ed.; All’insegna del Giglio: Firenze, Italy; pp. 410–414. (In Italian)
76. Rovida, A.; Locati, M.; Camassi, R.; Lolli, B.; Gasperini, P.; Antonucci, A. (Eds.) *Italian Parametric Earthquake Catalogue (CPTI15)*; version 4.0; Istituto Nazionale di Geofisica e Vulcanologia (INGV): Roma, Italy, 2022.
77. Forlin, P.; Gerrard, C.; Petley, D. Exploring Representativeness and Reliability for Late Medieval Earthquakes in Europe. *Nat. Hazards* **2016**, *84*, 1625–1636. [[CrossRef](#)]
78. De Marchi, P.M. (Ed.) *Castelseprio e Torba: Patrimonio dell’Umanità*; SAP Società Archeologica: Mantova, Italy, 2013.
79. Brogiolo, G.P. San Giovanni di Castelseprio. Architetture, Stratigrafie e Interventi dopo un Terremoto. *Eur. J. Post-Class. Archaeol. PCA* **2022**, *12*, 237–264.
80. Bugini, R.; Folli, L. Castrum Sibrium: Le Murature in Ciottoli del Complesso Basilicale di San Giovanni. *Sibrium Collana Studi Doc.* **2018**, *32*, 89–106.
81. Razzante, V. Analisi Archeometriche di Malte Storiche: Il Caso Studio Della Chiesa e del Cimitero di San Giovanni Evangelista in Castel Seprio. Master’s Thesis, University of Padua, Padua, Italy, 2023.
82. Dilaria, S.; Secco, M.; Bonetto, J.; Ricci, G.; Artioli, G. Making Ancient Mortars Hydraulic. How to Parametrize Type and Crystallinity of Reaction Products in Different Recipes. In *Conservation and Restoration of Historic Mortars and Masonry Structures*; Bokan Bosiljkov, V., Padovnik, A., Turk, T., Eds.; RILEM Bookseries; Springer Nature Switzerland: Cham, Switzerland, 2023; Volume 42, pp. 36–52, ISBN 978-3-031-31471-1.

83. Cescatti, E.; Rosato, L.; Valluzzi, M.R.; Casarin, F. An Automatic Algorithm for the Execution and Elaboration of Sonic Pulse Velocity Tests in Direct and Tomographic Arrangements. In *Structural Analysis of Historical Constructions. An Interdisciplinary Approach*; Aguilar, R., Torrealva, D., Moreira, S., Pando, M.A., Ramos, L.F., Eds.; Springer: Berlin/Heidelberg, Germany, 2019; pp. 716–724, ISBN 978-3-319-99440-6.
84. *G+D Computing Strand7*; R3.1.1 2022; Strand7 UK Limited: Cambridgeshire, UK, 2022.
85. Ministry of Infrastructures and Transportations. Ministerial Decree 17/01/2018, Aggiornamento Delle «Norme Tecniche per Le Costruzioni». 2018. Available online: <https://www.gazzettaufficiale.it/eli/id/2018/2/20/18A00716/sg> (accessed on 12 January 2024). (In Italian)

Disclaimer/Publisher’s Note: The statements, opinions and data contained in all publications are solely those of the individual author(s) and contributor(s) and not of MDPI and/or the editor(s). MDPI and/or the editor(s) disclaim responsibility for any injury to people or property resulting from any ideas, methods, instructions or products referred to in the content.